1958

Electron deficient bonding by elements of the third group

Elmer Louis Amma
Iowa State College

ELECTRON DEFICIENT BONDING BY ELEMENTS OF THE THIRD GROUP

by

Elmer Louis Amma

A Dissertation Submitted to the
Graduate Faculty in Partial Fulfillment of
The Requirements for the Degree of
DOCTOR OF PHILOSOPHY

Major Subject: Physical Chemistry

Approved:

Signature was redacted for privacy.

In Charge of Major Work

Signature was redacted for privacy.

Head of Major Department

Signature was redacted for privacy.

Dean of Graduate College

Iowa State College
1958

TABLE OF CONTENTS

INTRODUCTION

Shortly after the boron hydrides were discovered it was found that they presented a serious problem in valence in so far as the Lewis electron pair theory (1) was concerned. These compounds have fewer electron pairs than valence bonds and thus the term "electron deficient compounds" arose. For some time thereafter it was thought that the boron hydrides were unique; however, it is quite clear now that they are not. Dimeric trimethylaluminum, polymeric dimethylberyllium, tetramethylplatinum and many organo-metallic compounds belong to this class (2). As a matter of fact, interstitial compounds and even metals can be included with electron deficient compounds (3). With this knowledge at hand we can now make a general statement on electron deficient compounds.

Electron deficient compounds arise when an atom (usually a metal) with more low energy orbitals than valence electrons combines with an atom or group containing no unshared electron pairs. The metal atom then tends to make use of all its low energy orbitals to form delocalized bonds (4a,b).

Probably the best known and for a time the most controversial electron deficient compound was diborane. Doubt existed whether this molecule had the ethane (D_{3d}) structure or ethylene (D_{2h}) structure. After others (5) had made some convincing arguments, W. C. Price (6) convincingly showed, from a vibrational analysis of the perpendicular bands be-

tween 2600 cm.$^{-1}$ and 960 cm.$^{-1}$ that the molecule must have D_{2h} symmetry. This structure was later confirmed by electron diffraction (7) which gave the presently accepted bond parameters. However, even once the structure was known with certainty the bonding was not clearly understood. Pitzer (5c, 8) likened the bridge to a protonated double bond. At least the wording contradicts chemical (9) and proton magnetic resonance data (10) that the bridge protons are relatively negative. More important, the structure of the higher boron hydrides predicted from this idea are incorrect, primarily because all the low energy orbitals of boron are not utilized.

The bridge in diborane has been well described by a number of writers (11) in terms of three-center molecular orbitals. We shall here describe the bridge as a four-center four-electron problem similar to the description of Hamilton (12) and then indicate how the four-center orbitals are decomposed to the three-center orbitals. In these descriptions the wave functions are made up of a linear combination of the boron sp^3 tetrahedral orbitals and the hydrogen 1s orbitals.

Let us label the sp^3 hybrid bridge orbitals; on B_1 as χ_1 and χ_2, on B_2 as χ_3 and χ_4 and the hydrogen 1s bridge orbitals as ϕ_1 and ϕ_2; where the odd functions are above the plane defined by the borons and the external hydrogen atoms and the even ones below, Figure 1. Then we can easily derive the wave functions assuming no interaction between the ex-

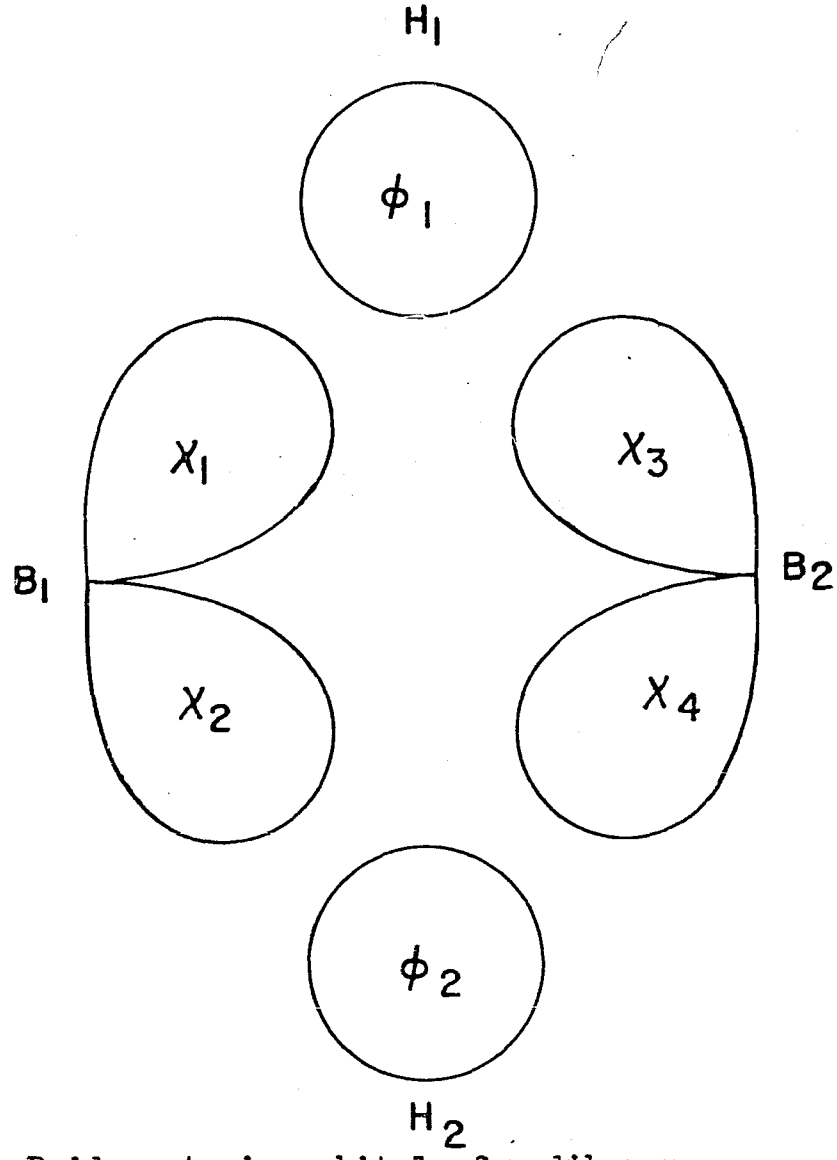

Figure 1. Bridge atomic orbitals for diborane
X's are boron sp^3 hybrid orbitals
ϕ's are hydrogen 1s orbitals

ternal boron-hydrogen bonds and the bridge. Further, the molecule is assumed to have D_{2h} symmetry and the normalization constants are neglected for simplicity. These wave functions along with the irreducible representations to which they belong are listed in Table 1.

Table 1. Molecular orbitals for diborane

Molecular orbitals	Irreducible representation	Comments
$\Psi_I = \chi_1 + \chi_2 + \chi_3 + \chi_4 + \phi_1 + \phi_2$	A_{1g}	Strongly bonding framework orbital
$\Psi_{II} = \chi_1 - \chi_2 + \chi_3 - \chi_4 + \phi_1 - \phi_2$	B_{3u}	Strongly bonding orbital with a nodal plane through plane defined by borons and external hydrogens
$\Psi_{III} = \chi_1 + \chi_2 - \chi_3 - \chi_4$	B_{1u}	Non-bonding
$\Psi_{IV} = \chi_1 - \chi_2 - \chi_3 + \chi_4$	B_{2g}	Non-bonding
$\Psi_V = \chi_1 - \chi_2 + \chi_3 - \chi_4 - \phi_1 + \phi_2$	B_{3u}	Antibonding
$\Psi_{VI} = \chi_1 + \chi_2 + \chi_3 + \chi_4 - \phi_1 - \phi_2$	A_{1g}	Antibonding

Now Ψ_I and Ψ_{II} are strongly bonding, Ψ_{III} and Ψ_{IV} are non-bonding and Ψ_V and Ψ_{VI} are strongly antibonding. The bonding, non-bonding and antibonding levels are, no doubt, sufficiently well separated that energetically the

four electrons (one from each boron and hydrogen atom) should be placed in the two bonding levels in accordance with the Pauli Principle. This closed shell situation leads directly to the diamagnetic character of diborane.

The four-center orbitals can readily be decomposed into three center orbitals as follows, with the same assumptions and notation as before.

Call $\Delta_I = \chi_1 + \chi_3 + \phi_1$ Bonding three-center orbital

$\Delta_2 = \chi_2 + \chi_4 + \phi_2$ Bonding three-center orbital

then $\Psi_I = \Delta_1 + \Delta_2$ belongs to A_{1g}: identical to four-center bonding A_{1g} orbital.

$\Psi_{II} = \Delta_1 - \Delta_2$ belongs to B_{3u}: identical to four-center bonding B_{3u} orbital

and $\Delta_3 = \chi_1 - \chi_3$ Non-bonding three-center orbital

$\Delta_4 = \chi_2 - \chi_4$ Non-bonding three-center orbital

then $\Psi_{III} = \Delta_3 + \Delta_4$ identical to four-center B_{1u} non-bonding orbital

$\Psi_{IV} = \Delta_3 - \Delta_4$ identical to four-center B_{2g} non-bonding orbital

also $\Delta_5 = \chi_1 + \chi_3 - \phi_1$ antibonding three-center orbital

$\Delta_6 = \chi_2 + \chi_4 - \phi_2$ antibonding three-center orbital

then $\Psi_V = \Delta_5 - \Delta_6$ identical to B_{3u} antibonding four-center orbital

$\Psi_{VI} = \Delta_5 + \Delta_6$ identical to A_{1g} antibonding four-center orbital

The point at hand is that for qualitative discussions it makes no difference whether we discuss the bridge as a four-center four-electron problem or as two three-center orbitals.

The structures of the higher boron hydrides (13, 14) have been determined by Lipscomb and his coworkers except for $B_{10}H_{14}$ which was discovered by Harker, Lucht and Kasper (15). Eberhardt, Lipscomb and Crawford (11b) have particularized the concepts outlined above to the higher boron hydrides describing the bonding in terms of these three-center bonds. Lipscomb (16) has applied the orbitals thus determined to the computation of dipole moments for some of the higher hydrides with mixed success.

Electron Deficient Methyl Bridges

At first glance the methyl bridge electron deficient compounds violate the "sacred" rule of organic chemistry that carbon can form only four electron pair bonds. However, as the discussion will later show this could be revised to say carbon uses four electron pairs in bonding but not necessarily to form electron pair bonds.

Tetramethylplatinum was the first methyl bridge electron deficient compound whose structure was surely known (17). In this case the molecular geometry is that of a distorted cube (T_d symmetry) where alternate corners are platinum and carbon atoms. Each platinum is bonded to three external methyl groups by normal Pt-C bonds and to three bridge carbons by electron deficient bonds. The platinum-platinum distance is 3.44Å, much too long for platinum-platinum bonding (platinum octahedral radius 1.30Å). The most reasonable interpretation of the bridge bonding is in terms of the platinum d^2sp^3 octahedral hybrid orbitals directed along the cube edges and one sp^3 hybrid orbital from each carbon directed toward the center of the cube.

By standard group theoretical methods (18) it can easily be shown that a linear combination of these carbon orbitals can belong to the irreducible representations: A_1 (non-degenerate) and T_1 (triply degenerate). The linear combination of platinum orbitals can belong to irreducible representations; A_1, T_1, E (doubly degenerate) and T_2 (triply degenerate). Therefore, the only combinations allowed under T_d symmetry between the carbon orbitals and the platinum orbitals belong to A_1 and T_1. Since each platinum atom and each bridge carbon contribute one electron to the bridge the diamagnetic character of tetramethylplatinum can easily be

understood by placing two electrons in A_1 and six electrons in T_1; both of which are bonding orbitals.

Unfortunately, the carbon atoms could not be accurately located in this structure because of the low scattering of x-rays of carbon relative to platinum. Their position had to be inferred from the isomorphous compound, trimethylplatinum chloride (17).

No one correctly predicted the geometry of trimethylaluminum dimer although attempts were made in this direction by a number of people. Pitzer and Gutowsky (19) knew it was a dimer, and from some infrared and Raman data they speculated that the relatively positive aluminum attracted the negative α carbon atom and the bonding forces were essentially dipole-dipole interactions. Further he speculated that the higher homologs did not dimerize because the aluminum atoms were too far separated by the CH_3 groups from the α carbon atoms for dipole-dipole interaction to be effective. He seemed to be uninhibited by the fact that the C-H dipole in most compounds seems to be in the other direction. Longuet-Higgins (20) speculated upon a trimer in spite of the vapor-density measurements. He also speculated in terms of a methylated double bond, but his conclusions were vague and his aluminum-aluminum distance of 1.9Å was unreasonably short.

The structure was determined by Lewis and Rundle (21) and from their results they laid a firm foundation for pre-

dicting the methyl bridge structures for the other light elements. The structure is as shown in Figure 2. The most significant quantities to note are the short Al-Al distance of 2.55Å (covalent radius of Al 1.26Å) and the sharp Al-C-Al angle of 70°.

Rundle describes the bonding in the trimethylaluminum dimer by asserting that the aluminum uses all its low energy sp^3 orbitals for bonding. Two of the aluminum atom sp^3 hybrid orbitals are used to form "normal" aluminum carbon bonds and the other two overlap with the sp^3 hybrid orbitals of the bridge carbons to form a four-center bridge bond. The sharp bridge angle is then a direct result of the tendency toward maximum overlap of the orbitals forming the bridge bond; this leads indirectly to the short aluminum-aluminum distance. A qualitative simple molecular orbital picture of this is as follows: assume the external aluminum-methyl bonds do not interact with the bridge bond and consider the bridge as a four center-four electron problem; further assume the molecular symmetry of D_{2h} (freely rotating methyl groups). Actually if the methyl groups were not freely rotating it would not alter the qualitative arguments to an appreciable extent. Let us label the bridge aluminum sp^3 orbitals on Al_1 as χ_1 and χ_2 and on Al_2 as χ_3 and χ_4 and the sp^3 carbon bridge orbitals as ζ_1 and ζ_2. The odd functions are above the

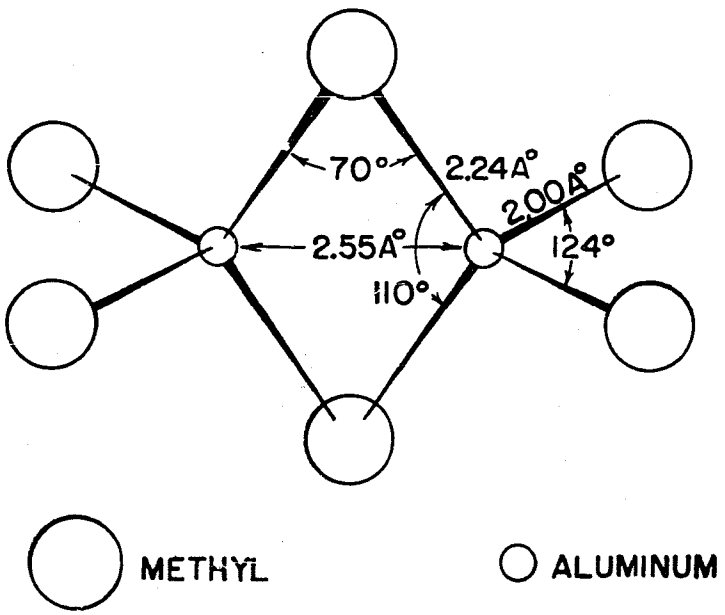

Figure 2. Molecular structure of trimethylaluminum

plane defined by the aluminum and the external carbon atoms; the even ones are below (Figure 3).

Then we can easily derive the molecular orbitals and their irreducible representations. They are listed in order of increasing energy in Table 2.

Again with four electrons and two strongly bonding orbitals the diamagnetic situation is easily understood.

The analogy that can be made between diborane and trimethylaluminum dimer is quite striking and shows clearly that the boron hydrides are by no stretch of the imagination unique.

Table 2. Molecular orbitals for trimethylaluminum dimer

Molecular orbitals	Irreducible representation	Comments
$\Psi_I = \chi_1 + \chi_2 + \chi_3 + \chi_4 + s_1 + s_2$	A_{1g}	Strongly bonding framework orbital
$\Psi_{II} = \chi_1 - \chi_2 + \chi_3 - \chi_4 + s_1 - s_2$	B_{3u}	Strongly bonding orbital with a nodal plane through the Al and external C atoms
$\Psi_{III} = \chi_1 + \chi_2 - \chi_3 - \chi_4$	B_{1u}	Non-bonding
$\Psi_{IV} = \chi_1 - \chi_2 - \chi_3 + \chi_4$	B_{2g}	Non-bonding
$\Psi_V = \chi_1 - \chi_2 + \chi_3 - \chi_4 - s_1 + s_2$	B_{3u}	Antibonding
$\Psi_{VI} = \chi_1 + \chi_2 + \chi_3 + \chi_4 - s_1 - s_2$	A_{1g}	Antibonding

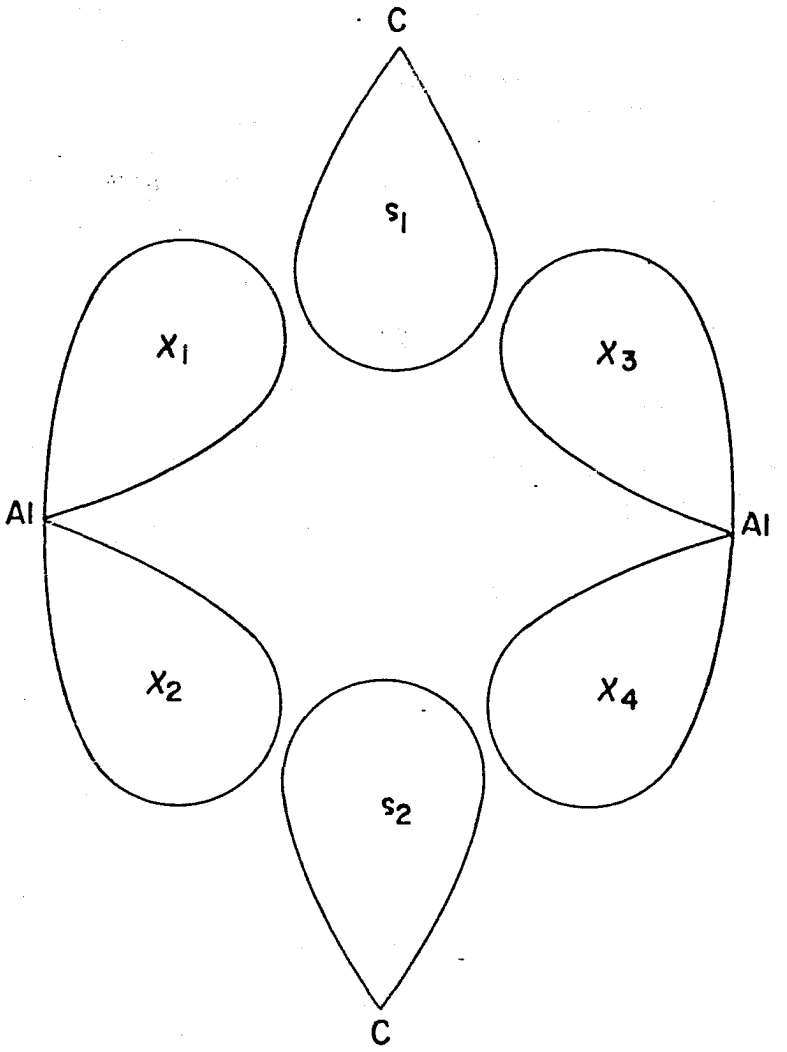

Figure 3. Bridge atomic orbitals for trimethylaluminum dimer
X's are aluminum sp^3 hybrid orbitals
s's are carbon sp^3 hybrid orbitals

The structure of the dimethylberyllium polymer was not correctly predicted by Pitzer and Gutowsky (19). All they could say was that the more electropositive element Be would more strongly attract the negative methyl. The structure was determined by Snow and Rundle (22) and the bonding can be readily understood in terms of the beryllium atoms making use of their sp^3 hybrid orbitals to overlap with bridge carbon sp^3 hybrid orbitals. The discussion applied above to dimeric trimethylaluminum can be applied here but one would then have to consider each bridge localized. The M-C-M angle here is even sharper than in trimethylaluminum dimer, 66°, as compared to 70° and the Be-Be distance is 2.09Å (Be covalent radius 1.06Å). All Be-C distances in this structure were found to be equal as would be expected on the basis of Rundle's (2) principles.

Now it is quite clear from the above principles and examples that if the metal atom becomes appreciably larger metal-metal repulsions will decrease the overlap between the metal orbitals and the bridge carbon sp^3 hybrid. Thus, with larger metal atoms the system has two choices: (1) to exist only as the monomer (2) to find another geometry and consequently a different type of electron deficient bonding.

Trimethylgallium (23) appears to be associated to a dimer but a somewhat weaker dimer than trimethylaluminum. This is not surprising since the covalent radius of Ga is experimentally the same as Al (1.26Å) (24) and the metal-metal repul-

sions in trimethylgallium probably are not very different from that in trimethylaluminum. However, the covalent radius of In is 1.44Å and indeed freezing point depression data (25) indicate a tetrameric structure for trimethylindium in benzene. The melting point of trimethylindium is also anomolously high (88°) compared to trimethylaluminum (15°). The vapor, in contrast, is only a plane trigonal monomer as determined by Pauling and Laubengayer (26). The object of part of this research was to determine the molecular geometry of trimethylindium in the solid phase and from this to infer the type of bonding.

Halogen Bridges

Halogen bridges occur quite frequently with the same metals as do methyl bridges. The geometry of halogen bridges and methyl bridges is quite similar but sufficiently different in certain respects to be indicative of different electronic structure.

The structures of Al_2Cl_6, Al_2Br_6, Al_2I_6 in the vapor phase have been found by Palmer and Elliot (27) by electron diffraction. The geometry of these molecules is strikingly similar to trimethylaluminum dimer except for two critical points. The metal-metal distance in dimeric aluminumtrichloride is much larger 3.64Å and the Al$\overset{Cl}{\diagdown\diagup}$Al angle is much larger, 92°, Figure 4. One can describe these structures as the

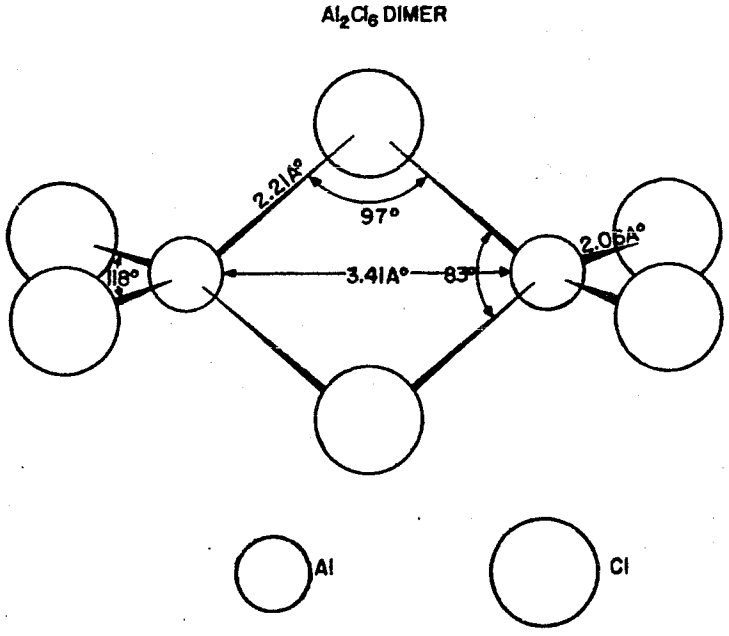

Figure 4. Structure of dimeric aluminum trichloride (vapor phase)

classical chemist has done for many years by discussing the bonding in terms of coordinate covalent links with resonance between the two forms.

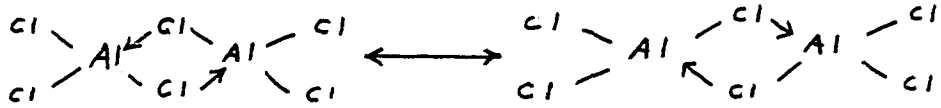

However, it is illuminating to discuss these in the same language as has been done for the trimethylaluminum dimer. In this way the difference between methyl electron deficient bridges and halogen bridges will become quite clear.

As in trimethylaluminum let us assume the Al-Cl bonds external to the bridge do not interact with the bridge bond and discuss the problem as an eight-electron four-center problem. The experimental Al-Cl-Al angle strongly implies pure p-bonding. Therefore, let us make molecular orbitals from the bridge sp^3 hybrid orbitals of aluminum denoted by χ_1, χ_2, χ_3, χ_4 and the p orbitals of each bridge chlorine denoted by $\omega_1, \omega_2, \omega_3, \omega_4$, Figure 5. Only two of the three p orbitals of each chlorine need to be considered since the other p orbitals belong to an irreducible representation independent of all the other bridge atomic orbitals (nonbonding orbital). If we now assume molecular symmetry D_{2h} and neglect the normalization constants the wave functions listed in Table 3 can be easily derived. They are listed in order of increasing energy, but it is difficult to decide

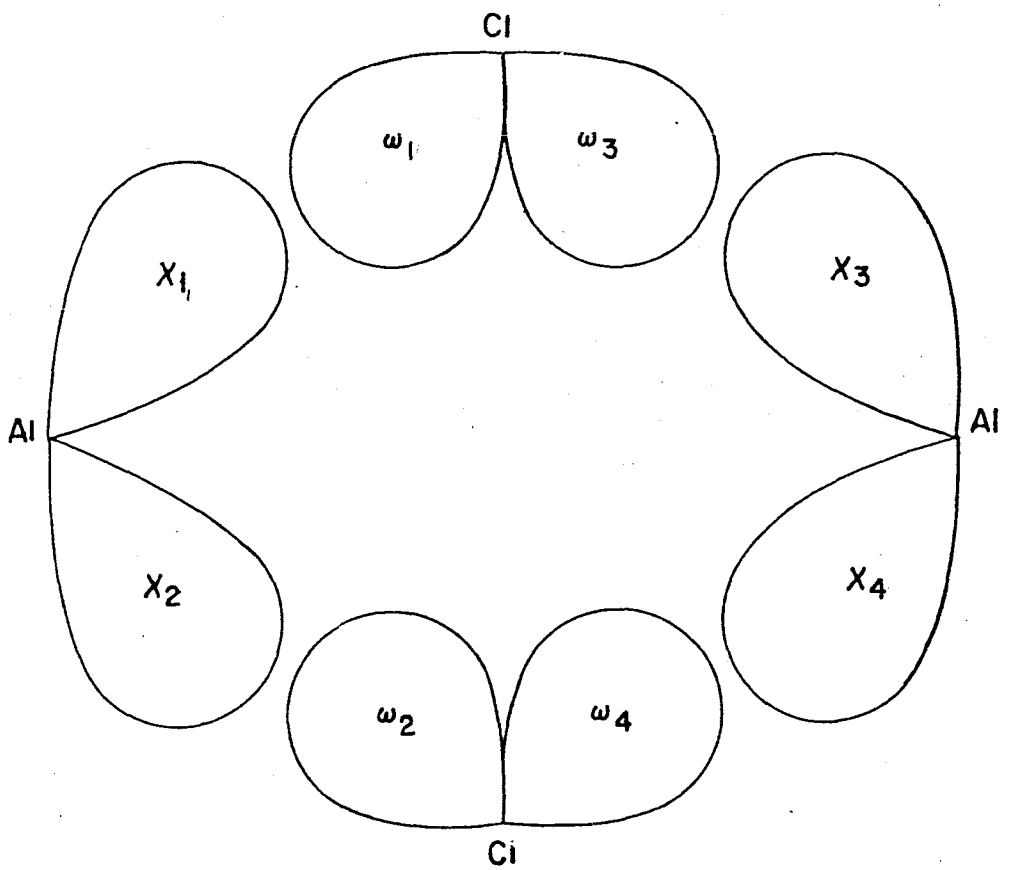

Figure 5. Bridge atomic orbitals for dimeric aluminum trichloride

X's are aluminum sp^3 hybrid orbitals
ω's are chlorine pure p orbitals

(other lobes of chlorine p orbitals not shown for simplicity)

Table 3. Molecular orbitals for Al_2Cl_6

Molecular orbitals	Irreducible representation	Comments
$\Psi_I = \chi_1+\chi_2+\chi_3+\chi_4 +\omega_1+\omega_2+\omega_3+\omega_4$	A_{1g}	Strongly bonding framework orbital
$\Psi_{II} = \chi_1-\chi_2+\chi_3-\chi_4 +\omega_1-\omega_2+\omega_3-\omega_4$	B_{3u}	Strongly bonding orbital with nodal plane through Al and external Cl atoms
$\Psi_{III} = \chi_1+\chi_2-\chi_3-\chi_4 +\omega_1+\omega_2-\omega_3-\omega_4$	B_{1u}	Strongly bonding orbital with nodal plane perpendicular to plane through Al and external Cl atoms
$\Psi_{IV} = \chi_1-\chi_2-\chi_3+\chi_4 +\omega_1-\omega_2-\omega_3+\omega_4$	B_{2g}	Strongly bonding
$\Psi_V = \chi_1-\chi_2-\chi_3+\chi_4 -\omega_1+\omega_2+\omega_3-\omega_4$	B_{2g}	Antibonding
$\Psi_{VI} = \chi_1+\chi_2-\chi_3-\chi_4 -\omega_1-\omega_2+\omega_3+\omega_4$	B_{1u}	Antibonding
$\Psi_{VII} = \chi_1-\chi_2+\chi_3-\chi_4 -\omega_1+\omega_2-\omega_3+\omega_4$	B_{3u}	Antibonding
$\Psi_{VIII} = \chi_1+\chi_2+\chi_3+\chi_4 -\omega_1-\omega_2-\omega_3-\omega_4$	A_{1g}	Antibonding

the order of B_{3u}, B_{1u}, B_{2g} states on a qualitative basis and they may well be interchanged.

We now have eight electrons to put into four bonding orbitals and again a closed shell electronic structure results. The B_{1u} and B_{2g} were non-bonding for trimethylaluminum since the sp^3 carbon orbitals could not belong to this representation.

From this description it is quite clear that there is nothing unique about electron deficient compounds. The only difference in a molecular orbital sense between trimethylaluminum and Al_2Cl_6 is in the atomic orbitals used to make up the bridge bond. It is interesting to note that this description of Al_2Cl_6 corresponds to one electron pair bond between each Al and Cl. The bonding in Al_2Cl_6 could have been equally well described in terms of two-center orbitals but not three-center orbitals, a characteristic of electron pair bonds.

A comparison similar to the one made above between dimeric trimethylaluminum and dimeric aluminumtrichloride can be made between polymeric dimethylberyllium and polymeric berylliumdichloride. The structure of berylliumdichloride was found by means of x-ray diffraction by Lewis and Rundle (28). The Be-Cl-Be angle was found to be 81° as compared to 66° for the Be-C-Be angle in dimethylberyllium. Again it seems reasonable, as in Al_2Cl_6, that the halogen uses nearly

pure p-orbitals for bridge bonding. The discussion of Al_2Cl_6 can then be readily extended to this case.

The structures of the dimeric gold trihalides (29), the dimeric dialkyl gold halides (30), the infinite chain palladous dichloride can all be understood in the very same language as dimeric aluminumtrichloride. In the gold and palladium compounds, however, the metal orbitals used in the bridge are the familiar d sp^2 hybrid orbitals.

The structure of trimethylplatinum chloride is also understandable in this same sense except now chlorine makes use of all three of its p orbitals in forming bonds with the d^2 sp^3 orbitals of platinum rather than only two as in dimeric aluminumtrichloride.

There seems to be a great deal of difference, however, between the vapor structure of some halides and their solid structure. As mentioned before, aluminum trichloride, aluminum tribromide and aluminum triiodide are dimers in the vapor phase, but aluminum trichloride (31) in the solid phase is that of a distorted $CrCl_3$ structure (32), i.e. the aluminum has a coordination number of six. It is a typical ionic layer lattice structure in spite of the fact that Raman data (33) indicated it was dimeric in the solid. Aluminum tribromide on the other hand retains the dimer molecule into the solid phase (34); unfortunately, the structure has not been suf-

ficiently well determined in the solid to compare distances and angles with the electron diffraction work on the vapor. The Raman data (33) are also consistent with a dimer in the solid for this compound. Barnes and Segel (35) have studied the electric nuclear quadrupole resonance of solid aluminum tribromide and have identified the Br^{79} and Br^{81} nuclear quadrupole resonance frequencies, and their interpretation of the observed frequencies is consistent with a dimeric molecule in the solid.

The crystal structure of aluminum triiodide is unknown but Barnes and Segel found a close correspondence between the resonance spectrum of $AlBr_3$ and AlI_3 (35, 36). Specifically, in $AlBr_3$ and AlI_3 the spectrum consists of three resonances for each isotope, two lines lying close together and differing by 1 per cent of the resonance frequency and the third about 15-20 per cent of the resonance frequency below the other two. The first two lines are attributed to crystallographically distinct halogen atoms, the halogens external to the bridge, and the lowest line is attributed to the bridge halogen. If AlI_3 is a dimer in the solid its melting point relative to $AlCl_3$ and $AlBr_3$ seems rather strange ($AlCl_3$ M.P. 193° at 2.5 atm; $AlBr_3$ M.P. 97°; AlI_3 M.P. 191°) (37).

For the trichlorides and tribromides of gallium and indium (38) the metal-metal distance is large enough for them to exist as dimers (as indicated by electron diffraction) in

the vapor in contrast to trimethylindium. This large indium-indium distance as compared to the necessary metal-metal distance for trimethylindium to exist as a dimer is probably due to two factors, a larger M-X than M-C distance and a broader M-X-M angle than M-C-M angle. It is somewhat peculiar that the electron diffraction data, poor as it may be, indicates that GaI_3 is a plane trigonal monomer but InI_3 is a dimer (38). This may be due to inaccuracies in the admittedly poor data. The poor data did not permit the determination of the conformation of these dimers. It seems reasonable to assume a molecule of D_{2h} symmetry as in Al_2Cl_6, and therefore one might expect the bonding also to be very similar.

The crystal structure of $InCl_3$ has been found by Templeton (39) and it is essentially an ionic layer structure very similar to solid $AlCl_3$. Some preliminary photographs taken in this laboratory indicate that $InBr_3$ may also have an ionic layer lattice. The crystal structures of $GaCl_3$, $GaBr_3$, GaI_3 and InI_3 are unknown. Barnes (36, 41) and his coworkers have studied the nuclear quadrupole resonance of $GaCl_3$, $GaBr_3$, GaI_3, $InBr_3$ and InI_3 in the solid state, and the same basic pattern as indicated above for $AlBr_3$ occurs for each isotope. From this he concludes that these compounds are all dimers in the solid. Greenwood and Worrall (42) have studied the electrical conductivity of the solid and liquid of $GaCl_3$, $GaBr_3$ and GaI_3 and conclude from a decrease of the electrical

conductivity in going from the solid to the liquid that the solid must be essentially ionic and the liquid contains the nonconducting dimeric molecules.

An interesting phenomenon was observed by Barnes. At liquid nitrogen temperatures in InI_3 the metal and the bridge halogen resonance disappears, but in GaI_3 only the metal resonance disappears. This is indicative of some sort of phase transition, the exact nature of which is not clear.

Other physical properties of these IIIB halides are quite interesting: $GaCl_3$ M.P. 77.9°, B.P. 201°, $GaBr_3$ M.P. 121°, B.P. 280°. These are quite consistent with dimeric molecules in the solid. But on the other hand: $InCl_3$ M.P. 586°, sublimes; $InBr_3$ M.P. 436°, sublimes; InI_3 M.P. 210°, GaI_3 M.P. 212°: these do not seem very consistent with molecular solids.

It is interesting also to note that AlI_3, GaI_3 and InI_3 all melt within 20° of one another. It seems as though it makes little difference which metal combines with the iodine.

Since the above discrepancies were found to exist a complete x-ray structure determination was undertaken on GaI_3 to resolve some of the above uncertainties. Both the nuclear quadrupole resonance and the conductivity measurements could only infer the structure on the basis of other known structures, and the necessary extrapolations may well have been unwarranted.

STRUCTURE OF TRIMETHYLINDIUM

Preparation and Properties of Trimethylindium

Trimethylindium was prepared by the method of Dennis, Work, Rochow and Chamot (25) by Dr. B. Zaslow and given to us in sealed tubes. This method of preparation consists of refluxing dimethylmercury with excess metallic indium for several days. The trimethylindium thus formed was then sublimed from the residue of metallic mercury and indum.

The pure compound (25) is a colorless solid, melting at 89.5°C, strongly birefringent and possibly existing in two crystalline modifications of which one is dominant. It is very reactive to water, oxygen and air. It is soluble in acetone, benzene, ether and carbon tetrachloride. The density as determined by pycnometric methods is 1.568g/c.c. Freezing point depression measurements of benzene solutions indicate a molecular weight of four monomeric units. In contrast to the analogous aluminum compound the etherate of trimethylindium is very unstable (44), but it forms a surprisingly stable (M.P. 66°C) trimethylamine adduct.

For single crystal x-ray structural determination trimethylindium was sublimed into capillaries on a vacuum line. Single crystals were grown by heating the capillaries in a water bath and allowing the bath to cool slowly. Single crystal x-ray photographs indicated the existence of a tetrag-

onal and a less stable, pseudo-hexagonal form of trimethylindium. The pseudo-hexagonal form was by far the least abundant of the two forms and was not investigated in this research. However, both forms were quite unstable in the x-ray beam and numerous crystals had to be examined in order to obtain the data necessary for a thorough structural investigation.

X-Ray Data

Crystals were found to grow in the capillary with the [001] direction, the [110] direction or the [010] direction parallel to the capillary axis. From crystals with the [110] direction parallel to the capillary axis hk0 and hhℓ intensity data were taken by means of timed exposures of 2, 5, 10, 15, 30 minutes and 1, 2, 4, 8, 16 hour duration. From crystals with the [010] direction parallel to the capillary axis okℓ precession data were taken by timed exposures as for the hk0 and hhℓ data. From crystals with the [001] direction parallel to the capillary axis Weissenberg equi-inclination photographs of reciprocal levels hk0, hk1 ...hk6 were obtained by a combination of multiple-film and timed exposure technique so that the intensity of a reflection could be estimated on more than one film. The precession data were corrected for Lorentz and polarization factors by means of a chart due to Waser (45). The Weissenberg data were cor-

rected for Lorentz and polarization factors by means of a table computed on the I.B.M. 604 from the function given by Cochran (46). Higher layer Weissenberg data were corrected for spot extension from a chart published by Phillips (47). All intensity data were estimated visually. Laue photographs were also taken of the hk0 and hhℓ zones.

Unit Cell and Space Group

Trimethylindium was found to be tetragonal with lattice constants (as determined by back reflection methods (48)),

$$a = b = 13.24 \pm .01 \text{ Å}$$
$$c = 6.44 \pm .01 \text{ Å}$$

with eight molecules per unit cell, $\rho_{cal.} = 1.88$ g/c.c., $\rho_{obs.} = 1.568$ g/c.c. The Laue class was observed to be $4/m\text{-}C_{4h}$ with the following systematic extinctions: for hk0 data; reflections absent for $h + k = 2n + 1$: for 00ℓ data; reflections absent for $\ell = 2n + 1$. This uniquely determined the space group to be $P4_2/n$ (49).

Determination of Atomic Positions

From the above lattice constants and the experimental density 6.7 formula units per unit cell were calculated. However, this leads one to suspect the experimental density is in error, and eight molecules per unit cell were assumed

in the analysis. These could be placed in the eight-fold set of general positions,

$$\pm \left[x,y,z;\ \tfrac{1}{2}-x,\ \tfrac{1}{2}-y,\ z;\ \tfrac{1}{2}-y,\ x,\ \tfrac{1}{2}-z;\ y,\ \tfrac{1}{2}-x,\tfrac{1}{2}-z\right] .$$

A Patterson projection onto the (001) plane was calculated using the Patterson function,

$$P(xyo) = \sum_{h=1}^{N}\sum_{k=1}^{N}\left[F^2(\bar{h}k0)+ F^2(hk0)\right] \text{Cos } 2\pi h\, x \text{ Cos } 2\pi ky$$

$$+ \sum_{h=1}^{N} F^2(h00) \text{ Cos } 2\pi hx + \sum_{h=1}^{N}\sum_{k=1}^{N}\left[F^2(\bar{h}k0)- F^2(hk0)\right] \text{Sin } 2\pi h$$

$$x \text{ Sin } 2\pi ky + \sum_{k=1}^{N} F^2(0k0) \text{ Cos } 2\pi ky$$

where $F^2(\bar{h}k0) = F^2(kh0)$.

The Patterson vector map is shown in Figure 6. With the origin of $P4_2/n$ at $\bar{1}$ the Patterson vectors can easily be derived and are shown in Table 4. The Patterson map can be interpreted with these vectors, assuming eight indium atoms per unit cell, to give the indium parameters x = .214, y = 0. No attempt was made to interpret indium-carbon vectors.

The conventional heavy heavy atom technique was then employed to find the carbcn atom parameters, i.e., structure factors (with James-Brindley scattering factors (50)) were calculated on the basis of the heavy atom positions and the

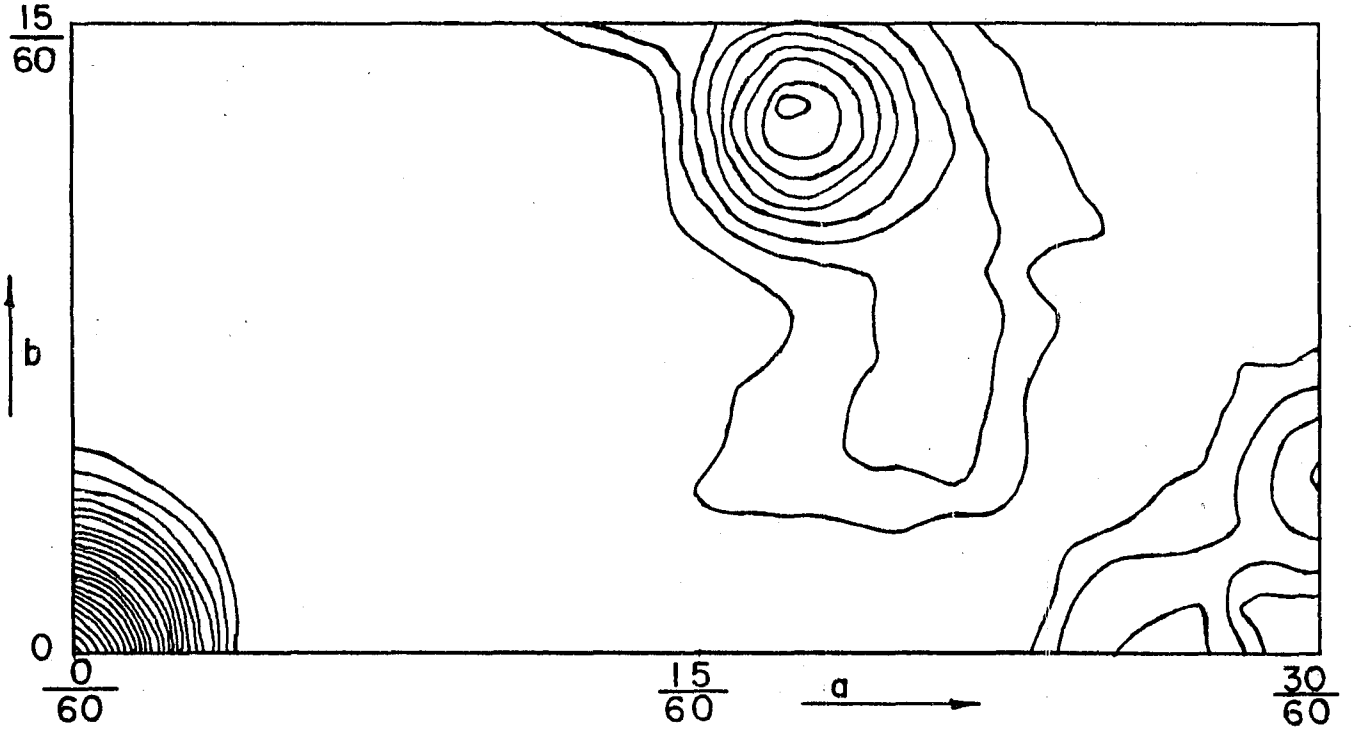

Figure 6. Patterson projection onto the (001) plane

Table 4. hk0 Patterson vectors

Multiplicity	Vector	Peak at
2	(2x, 2y)	26/60,0
2	($\frac{1}{2}$+ 2y, $\frac{1}{2}$- 2x)	30/60, 4/60
2	(-2x, -2y)	(34/60, 0)
4	($\frac{1}{2}$- x -y, -y+ x)	(17/60, 13/60)
4	($\frac{1}{2}$+ x- y, y+ x)	(43/60, 13/60)
and thus x = 13/60, y = 0		

signs thus determined were used as the signs of the Fourier amplitudes in the electron density analysis. An electron density projection onto the (001) plane was then computed using the function,

$$\rho(xy0) = \sum_{h=1}^{N}\sum_{k=1}^{N}\left[F(\bar{h}k0) + F(hk0)\right]\cos 2\pi hx \cos 2\pi ky$$

$$+ \sum_{h=1}^{N} F(h00)\cos 2\pi hx + \sum_{h=1}^{N}\sum_{k=1}^{N}\left[F(\bar{h}k0) - F(hk0)\right]\sin 2\pi hx$$

$$\sin 2\pi ky + \sum_{k=1}^{N} F(0k0)\cos 2\pi ky.$$

This projection seemed to be well resolved except for what appeared to be some anisotropic thermal motion of the heavy metal atom. Peak centers were located by Booth's (51) method and the results were as follows:

Atom	Parameters x	y
In	.214	.003
C_1	.141	.129
C_2	.075	.029
C_3	.333	.933

Structure factors were then calculated including all atoms [carbon atom scattering factors (52)] and a semilog plot of log F_c/F_o vs. $\sin^2\theta/\lambda^2$ was made. The slope of this graph gave the isotropic temperature factor of 4.92 and the intercept ($\sin^2\theta/\lambda^2 = 0$) gave the scale factor 8.71. With these quantities an R value

$$R = \frac{\sum_i \left| |F_o|_i - |F_c|_i \right|}{\sum_i |F_o|_i}$$

of .151 was obtained, usually considered good agreement for an early stage of structure determination.

It was decided to refine this projection by a difference synthesis (53), i.e., by computing a difference electron density projection where instead of $F_o(hk0)$, values of $[F_o(hk0) - F_c(hk0)]$ are used as Fourier coefficients, where F_c is a calculated structure factor based on spherical atoms corrected for thermal motion and F_o is the observed structure factor placed on the same scale as F_c. This type of Fourier analysis leads to characteristic map features that enable one: a) to decide on the direction an atom must be moved to-

ward the correct position, b) to observe directly anisotropic thermal motion and c) to make backshift corrections without additional computation. A difference electron density projection onto the (001) plane was computed with the above mentioned parameters, temperature factor and scale factor and is shown in Figure 7. Some rather surprising features were noted: (1) there is a relatively deep hole where the C_2 atom was placed, (2) there is a large positive region near the metal atom position and (3) the metal atom shows none of the features expected for anisotropic thermal motion. Attempts to improve the situation by shifting atoms proved futile. It was then decided that the C_2 atom had been placed at a false maximum and that it belonged very close to the metal atom in this projection. At this stage the original intensity data were carefully reexamined and a few small errors were found, errors that in most crystal structure determinations would make little difference.

The ordinary electron density projection onto the (001) plane was then recomputed (Figure 8) and the false maximum, indeed, disappeared. Therefore, C_2 had been incorrectly placed. A partial difference electron density projection was then computed by subtracting out only the metal atom contribution to the scattering. The electron density onto the (001) plane thus computed is shown in Figure 9. The C_2 atom was clearly resolved in this projection. Thus a preliminary set of x

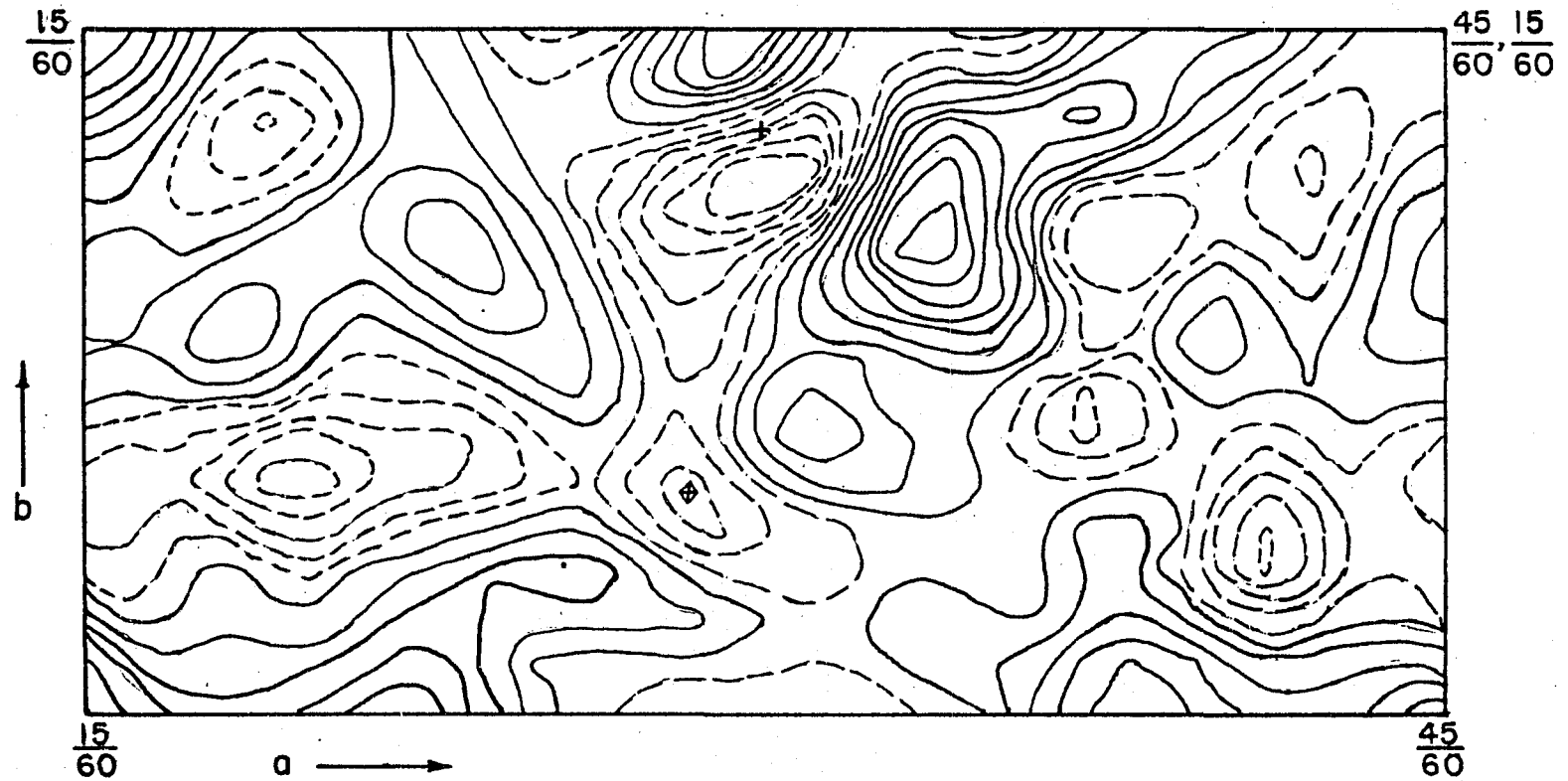

Figure 7. Difference electron density projection onto the (001) plane

+ Input position for metal atom Dotted lines negative contours
⊠ Input position for C_2 atom Solid lines positive contours

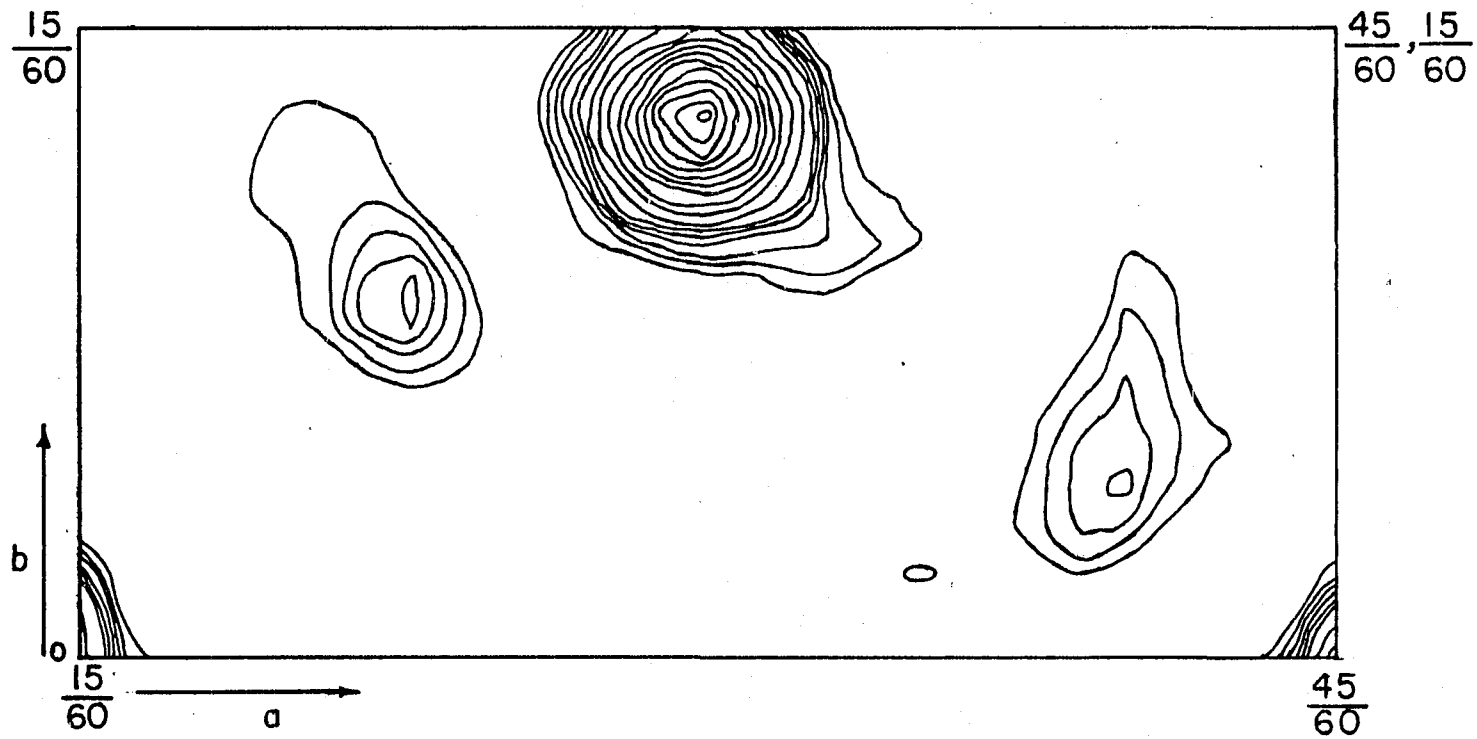

Figure 8. Electron density projection onto the (001) plane

Figure 9. Partial difference electron density projection onto the (001) plane (only the metal atom contribution to the scattering has been subtracted out)

X Input position of metal atom

and y parameters were obtained for all atoms, and they were as follows:

atom	parameters x	y
In	.214	.003
C_1	.143	.122
C_2	.185	.916
C_3	.319	.933

For these parameters R = .122.

By trial and error it was found that the metal-atom z parameter was approximately .411. Heavy atom techniques were then applied to the electron density projection onto the (110) plane in order to resolve the carbon atoms. However, this projection was poorly resolved due to overlapping of peaks, and all that could be ascertained from this projection was that the metal atom parameter of 0.411 was correct.

With the 0kℓ precession data an electron density projection onto the (100) plane was computed by heavy atom techniques. A slight asymmetry of the metal atoms in the y direction was noted indicating a change of origin was necessary to be consistent with the parameters from the electron density projection onto the (001) plane. The origin was shifted to 3/4, 1/4, $\overline{1/4}$ from $\bar{4}$ of $P4_2/n$ as given in the International Tables (49). The new representation of the space group and the general set of positions are summarized in Table 5. With this new origin an electron density projection onto the (100)

Table 5. Space group representation, general positions and structure factor relations

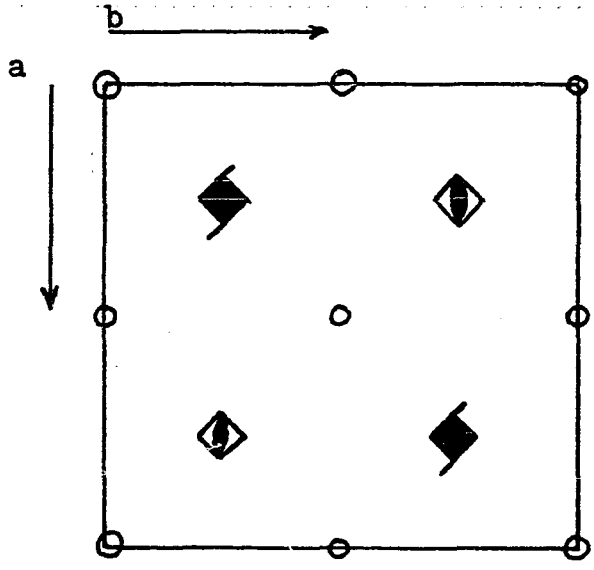

$P4_2/n$

Origin 3/4, 1/4, $\overline{1/4}$ from $\bar{4}$ of International Tables

General 8-fold set of positions:

$\pm$ (x,y,z; $\frac{1}{2}$- y,x,$\frac{1}{2}$+ z;$\frac{1}{2}$- x, $\frac{1}{2}$- y, z; y, $\frac{1}{2}$- x, $\frac{1}{2}$+ z)

$$F(hk\ell) = 2f_i \left[\cos 2\pi(hx+ky+\ell z) + \cos 2\pi(\bar{h}y+kx+\ell z+\frac{h+\ell}{2})\right.$$

$$+ \cos 2\pi(\bar{h}x+\bar{k}y+\ell z+\underline{h+k}/2)$$

$$\left.+ \cos 2\pi(hy+kx+\ell z+\underline{k+\ell}/2)\right]$$

$\underline{h+k = 2n \qquad k+\ell = 2n}$

$F(hk\ell) = F(\bar{h}\bar{k}\ell) = F(hk\bar{\ell}) \neq F(\bar{h}k\ell)$

$F(\bar{h}k\ell) = F(h\bar{k}\ell)$

$F(hh\ell) = F(\bar{h}h\ell)$

$\underline{h+k = 2n \qquad k+\ell = 2n+1}$

$F(hk\ell) = F(\bar{h}\bar{k}\bar{\ell}) = F(hk\bar{\ell}) \neq F(\bar{h}k\ell)$

Table 5. (Continued)

$F(\bar{h}k\ell) = F(h\bar{k}\ell)$

$F(hh\ell) = -F(\bar{h}h\ell)$

$\underline{h + k = 2n + 1}$

$k + \ell = 2n$

$h + \ell = 2n + 1$ $\qquad$ $A = B = 0$ if $\ell = 0$

$F(hk\ell) = F(h\bar{k}\bar{\ell}) = -F(hk\bar{\ell}) \neq F(\bar{h}k\ell)$

$F(\bar{h}k\ell) = -F(h\bar{k}\ell)$

$\underline{h + k = 2n + 1}$

$k + \ell = 2n + 1$

$h + \ell = 2n$

$A = B = 0$ if $\ell = 0$

$F(hk\ell) = F(\bar{h}\bar{k}\bar{\ell}) = -F(hk\bar{\ell}) \neq F(\bar{h}k\ell)$

$F(\bar{h}k\ell) = -F(h\bar{k}\ell)$

plane was computed via the heavy atom technique and is shown in Figure 10. The peak centers were located by Booth's method, where possible. The projection was not well resolved and very small changes in intensity considerably altered carbon peak positions. Symmetry arguments decided the correct molecular geometry including the carbon atoms, but for discussing bond

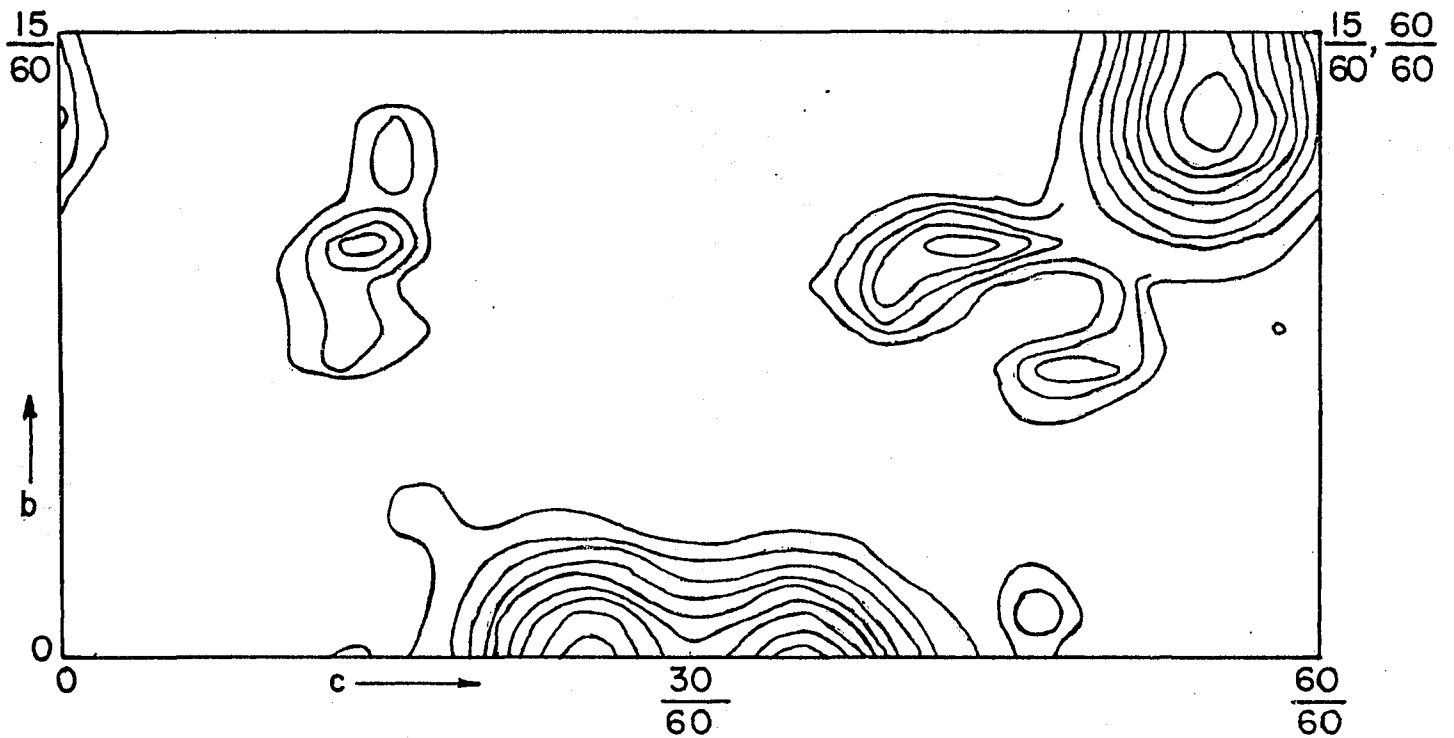

Figure 10. Electron density projection onto the (100) plane

angles and bond lengths this was clearly inadequate. Summary of the two dimensional results is in Table 6.

After considerable difficulty with decomposing crystals a crystal sufficiently stable for complete three-dimensional intensity data was obtained. Structure factors were calculated on the I.B.M. 604 for all the observed reflections and a semilog plot of log F_c/F_o vs. $\sin^2\theta/\lambda^2$ for each reciprocal level, hk0...hk6, was made in order to put all levels on a common scale.

Table 6. Summary of two-dimensional results

Closest In-In distance	5.22Å
Distance between In atoms related by the real 2-fold of the 4-fold inversion axis	6.76Å
Z separation of the two real two-folds of the 4-fold inversion axis	2.11Å
Distance between closest In atoms not in tetramer	5.67Å
In-C_3 (short bridge bond) distance	2.37Å
In-C_3 (long bridge bond) distance	2.97Å
In-C_3-In (bridge angle)	158°
In-C_1 (C_1 of next tetramer)	3.52Å
In-C_1 Bond length	2.17Å
In-C_2 Bond length	2.29Å

The electron density function,

$$\rho(xyz) = \sum_{h=1}^{N} \sum_{k=1}^{N} \sum_{\ell=1}^{N} F(hk\ell)\left[\cos 2\pi(hx+ky+\ell z) \pm \cos 2\pi(\bar{h}x+\bar{k}y+\ell z)\right]$$

$$+ F(\bar{h}k\ell)\left[\cos 2\pi(\bar{h}x+ ky+\ell z) \pm \cos 2\pi(hx+ \bar{k}y+\ell z)\right]$$

where the positive sign is used when $h + k = 2n$ and the negative sign when $h + k = 2n + 1$, was used to compute three dimensional electron density blocks. The blocks consist of a $4 \times 4 \times 4$ grid, where the grid spacing is 1/80 of the unit cell. The program on the I.B.M. 650 is such that the function is calculated for each of the 64 points in the block in one computation. Carbon atom positions were determined by computing one or more of these blocks beginning with the two-dimensional carbon atom parameters. One example of an electron density map computed by this means is shown in Figure 11.

Carbon atom peak centers were estimated from these blocks and gave the following parameters:

atom	parameters x	y	z
C_1	.143	.122	.233
C_2	.185	.946	.742
C_3	.340	.931	.198

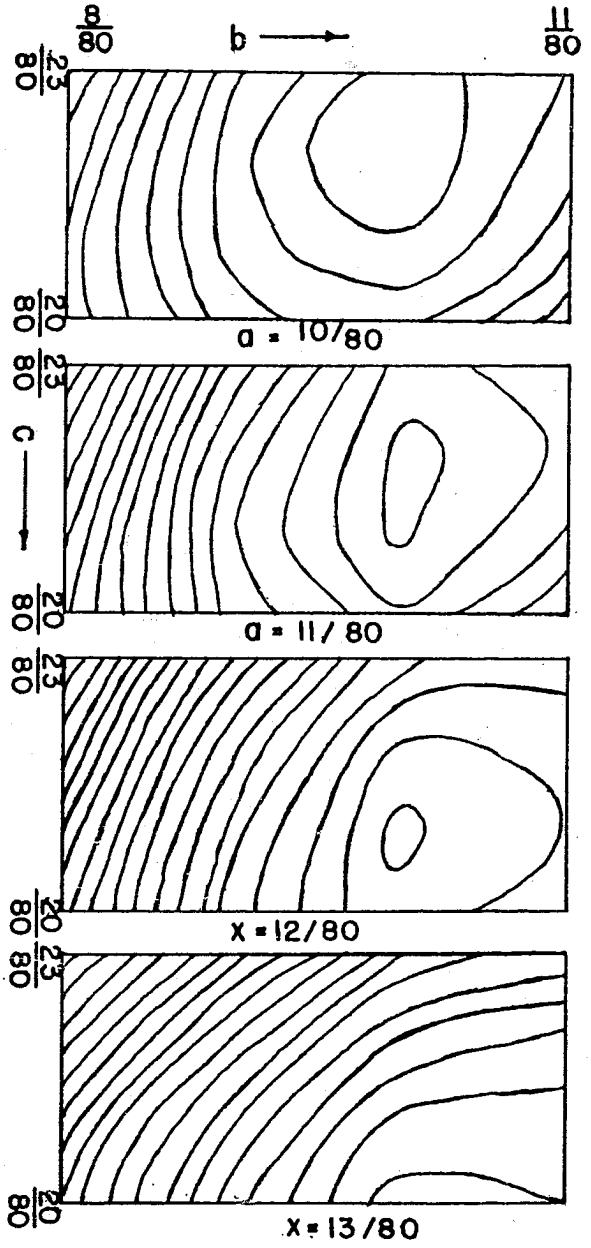

Figure 11. Electron density sections for C_1 atom

Refinement of Structure

The structure was refined by a least-squares method in which individual (but isotropic) atomic temperature factors, scale factors for each reciprocal level, as well as the positional parameters of the atoms are treated as variables. The program was written by Drs. Templeton and Senco for only orthorhombic symmetry but it was modified to treat monoclinic cases. Trimethylindium was reduced to monoclinic symmetry by doubling the positional parameters and including in the calculation those reflections which are independent by tetragonal symmetry but non-independent by monoclinic symmetry.

The function minimized by the program is $R = \sum_i \omega_i |F_o - F_c|_i^2$ where ω_i is a weighting factor. The variation of ω with F is shown in Figure 12.

Final results after four refinement cycles are shown in Table 7. The refinement was considered complete when parameters, temperature factors and the usual R factor ceased to change appreciably from one cycle to the next.

Interatomic distances were computed on the I.B.M. 650 with a program due to Templeton. Angles were computed manually. Standard deviations of bond lengths were computed by a formula due to Cruickshank (54). Interatomic distances and their accuracy are given in Table 8.

Final structure factors are tabulated in Table 9.

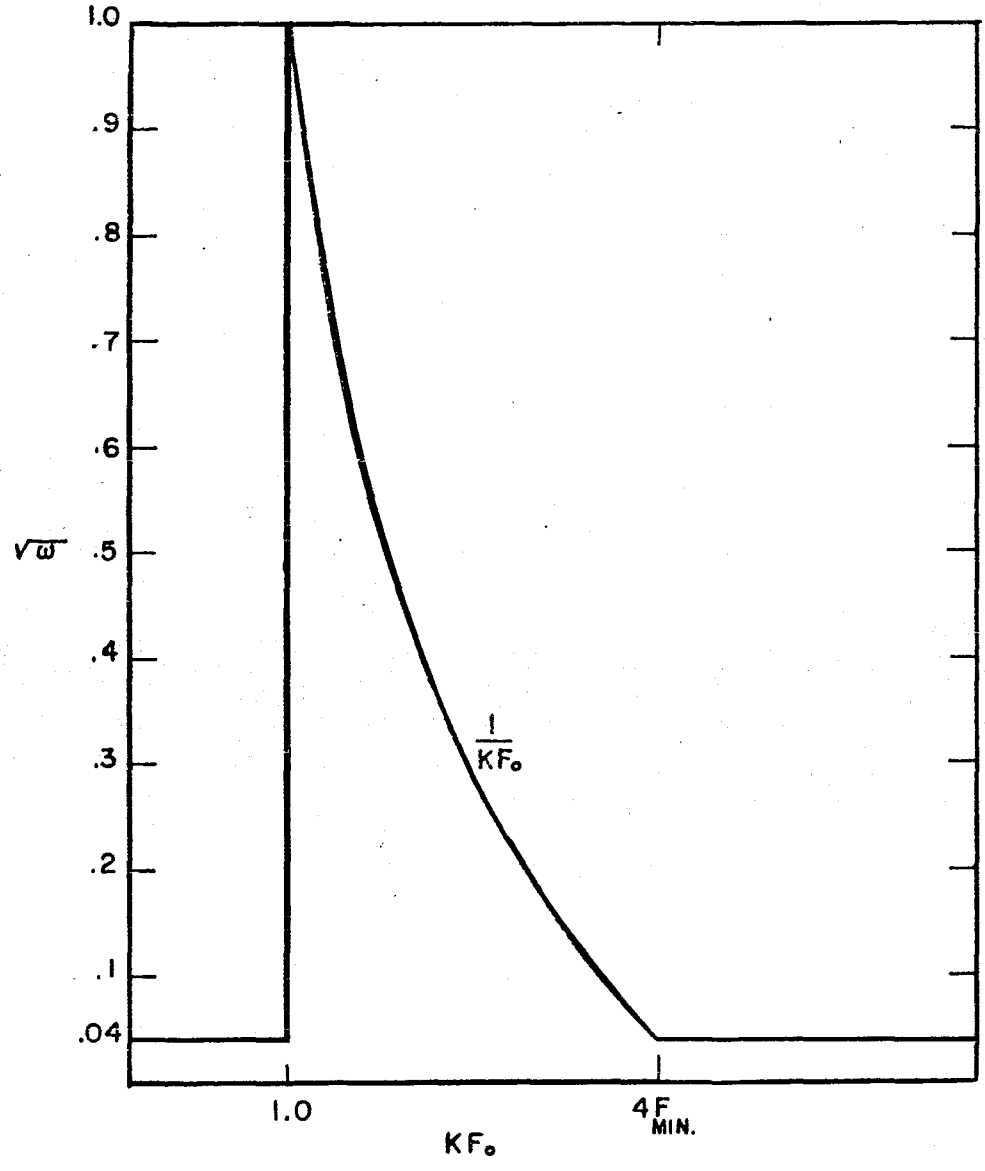

Figure 12. Variation of square root of weighting factor with observed structure factor. This weighting factor used in Templeton and Senco's least squares program

Table 7. Final parameters, standard deviations and atom temperature factors

Atom	x	y	z	σ_x	σ_y	σ_z	B/λ^2
In	.2140	.0038	.4124	.0002	.0002	.0005	10.3
C_1	.1420	.1282	.2684	.0027	.0027	.0070	9.29
C_2	.1710	.9620	.7086	.0028	.0027	.0067	8.94
C_3	.3422	.9282	.2785	.0028	.0028	.0071	9.37

$$R_1 = \frac{\sum_i \left| |F_o|_i - |F_c|_i \right|}{\sum_i F_{o\,i}} = 11.8\%$$

$$R_3 = \frac{\sum_i \omega_i |F_o - F_c|_i^2}{\sum_i |F_o|_i^2} = 8.57\%$$

Scale factors

$K_0 = 3.53$
$K_1 = 3.37$
$K_2 = 3.88$
$K_3 = 3.99$
$K_4 = 4.33$
$K_5 = 4.57$
$K_6 = 5.05$

Table 8. Bond distances and angles

In_1-C_3	2.15 ± .04Å	Short bridge bond within tetramer
In_2-C_3	3.11 ± .04Å	Long bridge bond within tetramer
In_1-C_1	2.12 ± .04Å	Short bridge bond to another tetramer
In-C_2	2.06 ± .04Å	Unbridged In-C distance
In_3-C_1	3.59 ± .04Å	Long bridge bond to another tetramer
In_1-In_2	5.235± .004Å	Closest In-In distance within tetramer
In_1-In_3	5.665± .004Å	Closest In-In distance between tetramers
In_1-In_4	6.79 ± .004Å	Distance across tetramer
C_3-C_3	3.78 ± .05Å	Bridge methyl contact distances within tetramer

Table 8. (Continued)

In-C-In	Bridge angle within tetramer is linear within experimental error
C_1-In-C_3	angle = 122°
C_2-In-C_3	angle = 117° "Monomer"
C_1-In-C_2	angle = 119°

Table 9. Final structure factors for trimethylindium

Structure factors positive unless designated otherwise

$F_c' = F_c/8$

Indices	KF_o	$F_c' e^{-B'S^2}$	Indices	KF_o	$F_c' e^{-B'S^2}$
(h00)					
4	46.6	49.5	5	46.6	-48.6
6	22.3	27.4	9	24.5	26.1
8	13.5	15.0	13	8.1	7.3
10	18.3	19.8	15	4.1	4.0
14	11.7	12.2			
18	4.3	3.9	(h40)		
			0	46.6	49.5
(h10)			2	14.3	-17.8
3	32.7	-36.3	4	40.2	41.8
5	20.3	25.3	6	6.8	7.9
7	27.7	-31.5	8	6.9	4.9
9	6.4	5.7	10	11.7	13.9
11	13.0	-12.5	14	6.9	6.1
(h20)			(h50)		
2	81.9	-82.2	1	17.1	-19.5
4	6.4	- 7.2	3	46.6	-47.4
6	24.5	-26.4	5	11.2	-11.6
8	17.4	-23.9	7	32.8	-40.3
10	3.1	- 3.6	11	15.5	-15.9
12	13.3	-13.3	13	5.4	- 3.7
16	6.6	- 5.7	15	4.4	- 3.3
			17	3.8	- 3.4
(h30)					
1	37.4	37.5			

Table 9. (Continued)

Indices	KF_o	$F_c' e^{-B' S^2}$	Indices	KF_o	$F_c' e^{-B' S^2}$
(h60)					
0	22.3	27.4	9	9.1	8.8
2	22.4	-25.9	13	2.7	2.1
4	9.5	12.1			
6	9.9	- 9.8	(h.12.0)		
10	4.8	4.6	2	16.8	-16.6
12	6.1	- 6.1	6	11.0	-10.8
14	5.9	5.3	8	6.2	- 5.3
			10	4.2	- 2.8
(h70)			12	6.2	- 5.0
1	25.7	31.1			
3	12.7	12.1	(h.13.0)		
5	29.9	34.2	3	4.0	- 1.0
7	3.1	1.9	7	5.7	- 6.0
9	17.2	19.9			
13	8.3	7.9	(h.14.0)		
			0	11.7	12.2
(h80)			4	11.0	9.1
0	13.5	15.0	8	4.5	4.1
2	18.9	-22.1	10	4.1	3.2
4	7.1	4.6	14	4.6	2.5
6	11.9	-12.6			
8	5.7	- 3.6	(h.15.0)		
12	7.9	- 8.2	7	6.0	- 4.3
16	2.8	- 2.9			
			(h.16.0)		
(h90)			2	7.6	- 6.8
1	14.2	-15.5	6	3.6	- 3.4
3	19.3	-22.0			
7	16.0	-17.3	(h.17.0)		
11	9.1	-10.0	5	2.8	2.9
(h.10.0)			(h.18.0)		
0	18.3	19.8	0	4.3	3.9
2	3.8	- 3.2			
4	15.6	19.1	(0.18.0)		
6	5.0	3.5			
8	6.4	7.5	(h01)		
10	9.3	7.8	3	18.3	15.7
14	5.6	4.9	4	10.9	12.5
			6	27.2	26.7
(h.11.0)			8	18.7	20.8
1	5.1	4.4	9	7.5	6.7
5	10.7	10.6	10	4.9	4.0

Table 9. (Continued)

Indices	KF_o	$F_c' e^{-B' s^2}$	Indices	KF_o	$F_c' e^{-B' s^2}$
12	13.6	14.1	6	16.7	15.9
13	5.2	5.5	7	11.6	11.4
16	5.5	5.5	8	8.4	9.2
18	4.2	0.4	9	10.8	11.6
			12	8.1	8.4
(h·1·1)			13	5.9	6.1
0	19.7	23.1			
1	17.2	17.6	(h51)		
3	11.8	11.9	1	27.0	-28.8
4	17.7	20.5	4	13.8	13.9
5	27.4	-31.8	5	29.9	-36.2
7	12.2	12.2	6	6.6	- 7.1
8	21.3	20.8	8	9.0	10.3
9	17.6	-18.6	9	22.3	-20.9
12	6.0	7.4	10	4.5	- 4.4
13	3.5	- 4.5	13	7.0	- 6.7
14	4.5	4.1			
			(h61)		
(h21)			0	27.2	-26.7
0	56.6	70.4	1	23.2	24.8
3	23.6	18.7	2	15.6	17.3
4	42.4	-42.6	4	14.8	-16.0
5	14.5	-15.8	5	17.4	-20.4
6	10.7	-14.4	11	6.7	- 8.4
7	11.6	-12.8	12	4.8	5.2
8	11.8	- 9.7			
10	14.6	-15.3	(h71)		
11	8.0	- 7.9	1	17.4	17.9
14	8.4	- 8.2	2	7.8	- 9.0
15	5.9	- 4.2	3	25.4	28.1
			4	7.5	7.3
(h31)			5	4.5	3.3
0	18.3	-15.7	6	6.3	- 6.4
3	33.3	37.4	7	23.2	23.3
6	19.6	-21.7	8	6.9	6.8
7	28.6	31.9	11	10.9	10.9
10	8.5	- 9.5	13	3.8	2.4
11	13.6	12.7			
			(h81)		
(h41)			0	18.7	-20.8
0	10.9	-12.5	2	11.1	10.5
1	6.2	- 7.2	3	19.3	19.9
2	41.1	42.4	4	13.8	-15.5
3	26.2	29.5	7	5.0	4.6

Table 9. (Continued)

Indices	KF_o	$F_c' e^{-B' s^2}$	Indices	KF_o	$F_c' e^{-B' s^2}$
8	4.7	- 3.7	(h·13·1)		
9	4.6	4.6	0	5.2	- 5.5
10	5.4	- 6.1	2	5.9	- 5.0
13	4.6	4.2	5	4.9	- 4.0
14	5.9	- 4.5	6	6.0	- 5.8
			10	4.2	- 2.8
(h91)					
0	7.5	- 6.8	(h·14·1)		
1	13.2	-12.5	2	9.9	9.6
2	5.5	- 4.7	6	5.1	5.6
3	7.0	- 5.0	8	4.3	2.5
5	16.3	17.7			
6	10.2	- 9.6	(h·15·1)		
9	11.2	-11.7	4	3.9	3.2
10	5.7	- 4.5			
			(h·16·1)		
(h·10·1)			0	5.5	- 5.5
0	4.9	- 4.0	4	4.4	- 4.5
1	14.7	-15.2			
2	14.7	18.3	(h·18·1)		
5	6.2	- 6.1	0	4.2	- 0.4
6	10.5	10.1			
8	5.1	5.1	(h02)		
10	3.9	2.0	0	9.6	11.6
11	3.8	- 2.9	3	31.4	-19.4
12	5.3	5.5	4	35.5	28.9
			5	13.5	12.6
(h·11·1)			6	3.4	4.9
1	7.0	5.9	7	3.5	3.4
2	5.8	5.0	8	7.8	6.1
3	10.2	7.8	10	10.8	11.5
4	9.1	8.8	11	11.0	9.9
7	9.8	9.1	13	4.4	- 4.3
8	5.5	6.4	14	4.6	4.3
11	4.2	4.0			
			(h12)		
(h·12·1)			0	31.0	32.9
0	13.6	-14.2	3	20.0	-13.7
1	3.3	- 2.9	4	4.5	3.6
3	4.6	4.9	6	39.9	38.9
4	10.9	-11.9	7	13.6	-14.3
6	4.7	- 2.7	9	6.3	5.0
8	4.4	- 4.8	10	18.2	18.8
10	5.9	- 4.7	11	6.1	- 5.0

Table 9. (Continued)

Indices	KF_o	$F_c' e^{-B' S^2}$	Indices	KF_o	$F_c' e^{-B' S^2}$
(h22)					
2	28.6	-22.7	2	17.3	-14.6
3	38.1	-36.8	3	37.6	-36.2
4	3.8	- 2.8	4	6.1	7.2
6	14.0	-13.4	5	5.5	- 6.1
7	12.0	-11.6	7	14.3	-13.7
8	5.6	- 4.4			
9	14.0	-14.3	(h72)		
12	6.9	- 7.1	0	3.5	3.5
13	8.8	- 9.6	1	3.9	6.0
			2	5.7	5.2
(h32)			4	9.5	-10.1
0	31.4	-19.5	5	13.5	13.0
2	10.5	- 9.9	6	14.8	13.6
4	33.9	-32.5	8	6.6	- 7.6
5	15.0	16.3	9	7.5	8.8
6	5.6	6.3	10	7.4	7.9
7	6.2	- 5.2			
8	22.1	-23.4	(h82)		
9	10.8	11.0	0	7.8	6.1
12	6.8	- 7.2	1	32.0	31.4
			2	9.6	-11.7
(h42)			4	5.5	4.8
0	35.5	28.9	5	5.8	18.3
4	15.5	10.2	7	7.7	6.4
5	29.3	29.0	9	5.9	3.9
7	13.2	12.8	11	8.5	8.1
9	6.3	5.1			
11	13.2	13.2	(h92)		
			1	6.6	- 5.1
(h52)			2	5.1	- 2.3
0	13.5	12.6	3	8.7	- 6.8
1	13.3	-14.2	4	13.9	-13.6
2	17.1	16.0	7	9.3	- 9.1
3	13.6	-13.6	8	11.8	-11.3
4	6.8	- 6.8	12	5.1	- 4.7
5	4.2	5.7			
7	13.8	-13.9	(h·10.2)		
8	7.2	- 9.8	0	10.8	11.5
10	7.8	9.0	3	16.2	-16.7
11	6.9	- 6.4	4	6.5	6.4
			7	6.5	- 5.8
(h62)			9	4.2	- 4.7
0	3.4	4.9			

Table 9. (Continued)

Indices	KF_o	$F_c' e^{-B'S^2}$	Indices	KF_o	$F_c' e^{-B'S^2}$
(h·11·2)			(h23)		
0	11.0	9.9	5	19.4	-20.7
1	4.6	4.1	7	5.1	- 4.9
2	9.8	8.8	11	11.1	-11.9
5	6.2	5.6	15	7.5	- 5.5
6	12.0	12.0			
10	7.6	6.6	(h33)		
			0	24.6	-22.3
(h·12·2)			2	35.7	-34.0
1	9.7	10.4	6	23.4	-27.6
2	6.7	- 7.6	10	11.2	-13.2
5	5.9	5.7			
6	4.2	- 3.3	(h43)		
			0	4.0	2.3
(h·13·2)			3	27.7	34.3
0	4.4	- 4.3	5	6.4	7.8
3	4.2	- 3.3	7	12.4	12.4
4	12.7	- 8.4	9	10.9	11.7
(h·14·2)			(h53)		
0	4.6	4.3	0	7.9	7.2
1	4.9	5.4	1	4.9	4.4
4	5.3	4.4	4	16.2	18.8
			6	8.4	- 9.6
(h·15·2)					
2	4.8	4.1	(h63)		
6	5.9	4.9	1	37.6	-38.7
			5	20.9	-20.0
(h03)			7	11.2	-12.0
1	29.2	-25.6	9	8.2	- 8.0
3	24.6	22.4	15	5.1	- 5.4
4	4.0	- 2.5			
5	7.9	- 7.3	(h73)		
9	7.1	7.4	4	10.4	11.4
11	4.8	- 5.9	6	8.7	- 9.1
13	7.2	6.8	8	11.6	11.4
(h13)			(h83)		
0	29.2	25.6	5	5.6	4.4
4	51.1	44.6	7	7.6	11.2
8	23.9	25.7	9	6.4	8.6
12	8.5	8.1			
			(h93)		
			0	7.1	- 7.4

Table 9. (Continued)

Indices	KF_o	$F_c' e^{-B' S^2}$	Indices	KF_o	$F_c' e^{-B' S^2}$
2	8.9	- 9.1	3	9.3	10.0
6	11.8	-12.4	5	4.6	- 3.1
10	8.8	- 8.3	6	23.6	22.1
			7	9.2	10.4
(h·10·3)			10	10.3	9.7
1	17.6	-15.9			
5	13.4	-11.5	(h24)		
11	5.1	- 4.4	2	21.5	18.5
			3	16.3	-18.2
(h·11·3)			6	21.5	9.6
0	4.8	5.9	7	4.8	5.0
2	6.0	4.1	8	5.8	4.6
4	7.1	9.7	9	5.5	- 5.9
8	9.3	9.1	12	6.1	5.6
12	5.4	4.5	13	4.8	- 5.7
(h·12·3)			(h34)		
3	8.8	8.7	0	11.8	-11.3
			1	10.2	- 8.2
(h·13·3)			2	7.0	- 5.6
0	7.2	- 6.8	4	19.5	-20.4
2	6.7	- 5.6	5	13.8	-12.8
6	8.2	- 7.3	8	14.0	-12.7
10	5.1	- 4.8	9	7.2	- 8.7
			12	6.0	- 4.1
(h·14·3)					
3	4.7	4.4	(h44)		
			0	17.9	-19.2
(h·15·3)			1	24.4	26.4
2	6.0	2.9	2	2.9	1.9
4	6.0	4.4	4	6.9	- 8.7
			5	14.9	12.8
(h04)			7	5.2	6.2
0	20.8	-17.0	9	5.9	4.5
1	15.0	15.5	10	4.1	- 3.0
3	11.8	-11.4	11	5.8	7.3
4	17.9	-19.3			
5	7.9	7.2	(h54)		
6	5.7	- 5.1	0	7.9	7.2
8	3.3	- 4.5	1	9.7	9.2
10	8.6	- 8.7	2	8.3	8.9
			3	12.2	11.7
(h14)			6	11.4	10.9
0	15.0	15.5	7	11.5	11.1

Table 9. (Continued)

Indices	KF_o	$F_c' e^{-B'S^2}$	Indices	KF_o	$F_c' e^{-B'S^2}$
11	4.2	5.4	4	3.9	1.6
			6	6.0	6.4
(h64)					
0	5.7	- 5.1	(h·12·4)		
2	7.6	9.9	1	6.6	5.7
3	17.7	-18.3	2	6.1	6.1
4	9.3	- 5.0	5	4.4	3.4
5	4.8	- 5.1	6	3.6	3.1
9	6.5	- 7.4			
			(h·13·4)		
(h74)			4	4.3	- 4.5
4	4.1	- 3.1			
5	9.6	-10.5	(h05)		
6	5.9	7.9	2	16.9	-21.0
8	5.3	- 4.4	3	6.3	3.6
9	7.4	- 7.4	8	8.5	- 8.7
10	4.1	4.6	12	6.3	- 7.5
(h84)			(h15)		
0	3.3	- 4.5	1	5.5	4.9
1	17.7	15.6	4	5.8	6.4
2	9.1	8.8	5	13.0	13.2
5	11.8	10.8	7	4.9	- 4.9
7	5.2	5.0	8	6.3	5.5
8	4.1	2.4	9	6.9	8.3
9	4.5	3.3			
11	4.3	4.6	(h25)		
			0	16.9	20.9
(h94)			3	3.8	3.4
1	3.7	4.1	4	15.1	15.9
3	5.3	5.7	5	5.4	- 3.5
4	6.1	- 6.9	6	4.7	2.9
7	6.1	7.3	8	5.0	4.5
8	6.6	- 7.5	10	6.1	7.3
(h·10·4)			(h35)		
0	8.6	- 8.7	0	6.3	- 3.6
1	3.6	1.9	3	11.7	-13.1
3	7.0	- 9.0	6	6.8	- 6.1
4	6.0	- 5.6	7	13.2	-13.0
7	4.9	- 4.0	11	5.8	- 6.5
(h·11·4)			(h45)		
2	4.5	5.2	2	14.7	-16.5

Table 9. (Continued)

Indices	KF_o	$F_c' e^{-B'S^2}$	Indices	KF_o	$F_c' e^{-B'S^2}$
3	7.1	7.2	5	4.3	- 4.4
6	4.9	- 5.8	7	7.9	8.0
12	6.4	- 3.9			
			(h26)		
(h55)			2	13.1	15.0
1	9.3	8.4	6	6.1	6.5
5	14.2	13.9	8	5.8	5.4
8	5.3	3.0			
9	9.5	9.9	(h36)		
			1	5.9	- 6.1
(h65)			5	9.8	-10.7
1	6.7	- 6.5	9	6.9	- 7.1
2	6.9	- 7.3			
4	5.8	6.7	(h46)		
5	6.8	- 5.6	0	11.4	-11.3
			4	8.9	- 9.0
(h75)					
3	9.4	- 9.8	(h56)		
			1	6.0	5.0
(h85)			3	9.0	9.6
0	8.5	8.8	7	9.0	9.4
3	6.0	5.4			
4	5.4	6.9	(h66)		
			0	5.5	- 5.3
(h95)			2	6.1	6.9
1	5.4	5.5			
5	8.6	8.5	(h76)		
			1	6.8	- 6.6
(h·10·5)			5	9.4	0.3
2	7.3	- 9.0	5	4.5	- 8.6
6	6.2	- 4.0			
			(h86)		
(h·12·5)			0	4.1	- 4.1
0	6.3	7.5	2	5.8	5.9
4	6.4	5.6			
			(h96)		
(h06)			3	6.5	5.8
0	18.1	-19.4			
4	11.4	-11.3	(h·10·6)		
6	5.5	- 5.3	0	5.1	- 5.7
8	4.1	- 4.1			
10	5.1	- 5.7			
(h16)					
3	5.3	7.2			

Discussion

Trimethylindium is a tetramer (Figure 13) or pseudo-tetramer with the geometry of a tetrahedron flattened along a four-fold inversion axis and related to its neighbors by centers of symmetry. The nearest metal atoms, within the tetramer, (Table 8, In_1-In_2, 5.24Å) are bonded together by linear, asymmetric, electron-deficient methyl bridges with a short metal to carbon (In_1-C_3) distance of 2.15Å and a long carbon to metal (In_2-C_3) distance of 3.10Å. The metal atoms of one tetramer are bonded to metal atoms of another tetramer (In_1-In_3, 5.66Å) by essentially linear, asymmetric, electron-deficient methyl bridges with a short metal to carbon distance (In_1-C_1) 2.12Å and a long carbon to metal distance (In_3-C_1) of 3.59Å. The latter long carbon to metal distance is 0.49Å longer than similar bonds within the tetramer, hence the tetramers appear to be weakly linked and are not true molecules.

Since the sum of the van der Waals radii of methyl (2.0Å) and indium (about 2.2Å (24)) is approximately 4.2Å, it seems reasonable that even the longest bridge bond (3.59Å) is indicative of a significant interaction beyond the usual van der Waals interaction. One could possibly dispute the use of a van der Waals radius derived from the packing of hydrocarbons for this case but a contraction of 0.6Å does not seem very likely. Other evidence to support the long, external

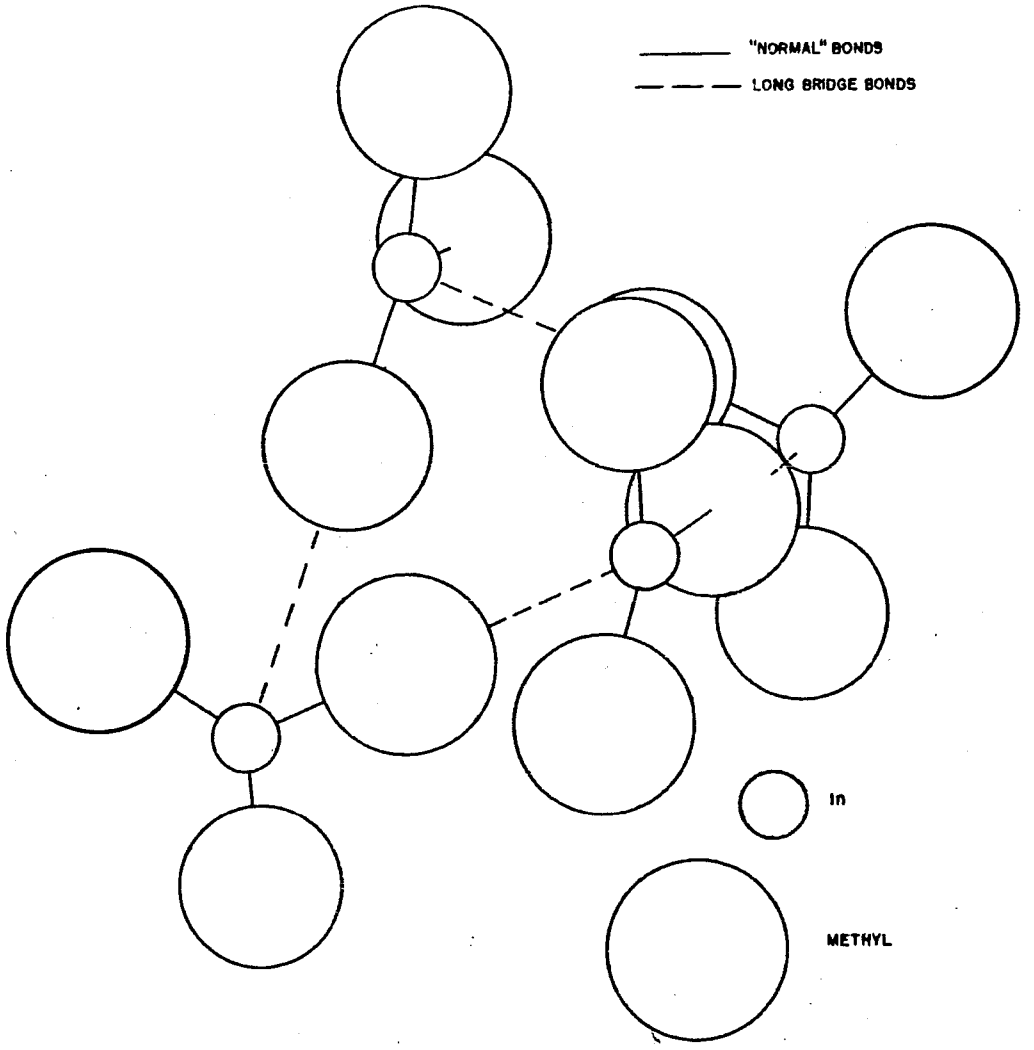

Figure 13. Tetramer of trimethylindium
(bonds to neighboring tetramers not shown)

to the tetramer, bridge bond is found by making a scale model. The only apparent reason for the flattened tetramer is that the long external bridge bond supports the tetramer, for the free tetrameric molecule could assume a planar configuration with little or no distortion of bonds. It is also to be noted that the structure is rather open and more efficient packing could exist if the external bridge bonds were not demanded.

The metal-metal distance across the tetrahedron (distance between atoms related by C_2 of S_4) is 6.79Å and the height of the tetrahedron (separation between sets of atoms related by C_2) is 2.09Å.

The configuration of carbon atoms about a metal atom is that of a distorted elongated trigonal bipyramid with the metal atom in the center, the "normal" metal to carbon bonds extending from the center of the equilateral triangle to the vertices and the long bridge bonds extending from the metal atom to the apices (Figure 14). If one considers only the "normal" bonds the configuration of carbon atoms about the metal atom is essentially trigonal as is the monomer in the vapor as determined by Pauling and Laubengayer (26) by electron diffraction.

Pauling and Laubengayer determined the indium-carbon distance to be 2.16 $\pm$ .04Å and the carbon-indium-carbon angle to be 120° $\pm$ 2° for the most probable model.

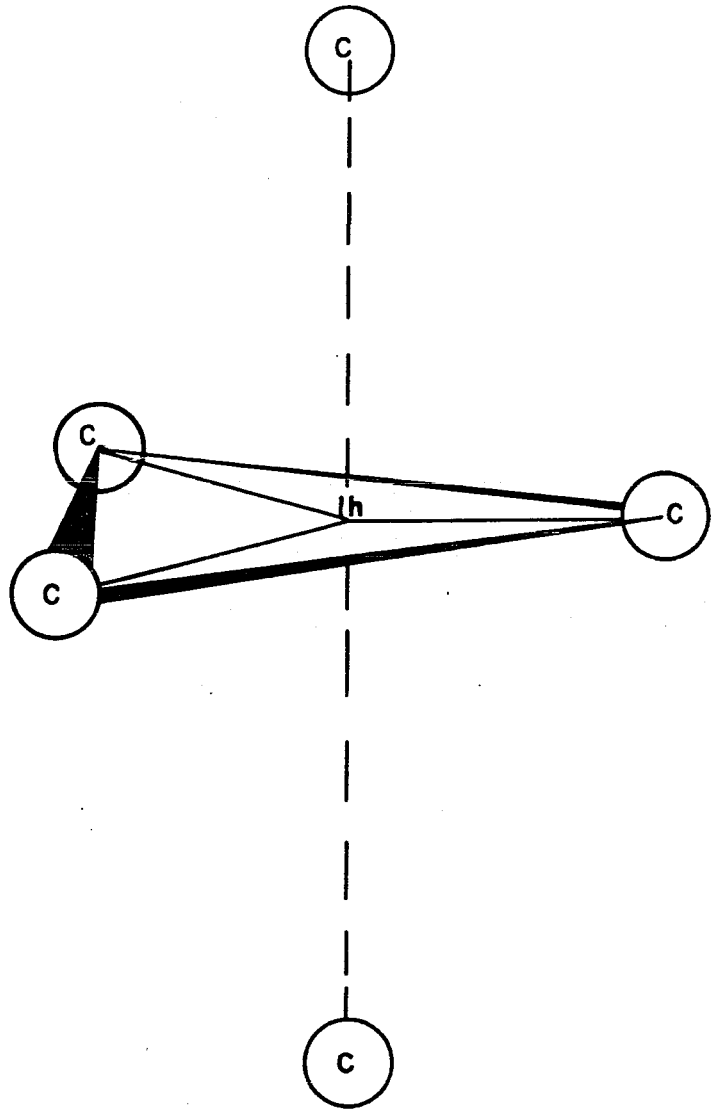

Figure 14. Local configuration of carbon atoms about a particular metal atom (idealized)
C---I---C angle is experimentally 163° not 180°

It is to be noted that the free, non-bridged, indium carbon distance (In_1-C_2, 2.06Å) is 0.1Å shorter than the indium carbon distance given by Pauling and Laubengayer. This difference may be significant as Cruickshank's (54) significance test indicates. This test is, if δl is the difference between two bond lengths and σ is the standard deviation of a particular bond, then, if

$\delta l \leq 1.645\sigma$ the difference is not significant,

$2.327\sigma > \delta l > 1.645\sigma$ the difference is possibly significant,

$3.090\sigma > \delta l > 2.327\sigma$ the difference is significant.

Using the x-ray standard deviation of .04Å, then 2.327σ = .093Å and the observed difference is 0.1Å. It would be tempting to say that the difference is significant but it may not be because the σ value is perhaps somewhat higher due to the reduction of symmetry in the refinement. The electron diffraction estimate of error is also probably an underestimate because of the breakdown of the Born approximation for heavy atoms. There also has been recent discussion (55a) that the method of Hughes (55b) for estimating standard deviations from least squares calculations underestimates the error as compared to Fourier methods of estimating error.

A point to be noted is the temperature factors, (B/λ^2) (Table 8) for all atoms seem to be quite large, perhaps twice as large as that found in most structures. This is perfectly

consistent with the physical property that trimethylindium can be sublimed easily at room temperature.

A possible interpretation of the bonding in pseudo-tetrameric trimethylindium is to assume that the metal atom is trigonally hybridized (as indicated by the geometry) and the bridge carbon atom is at least partially trigonally hybridized. Then the bridge bonding is through the pure p_z orbitals of the metal and carbon atoms. This would give rise to a five-center four-electron problem (Figure 15a). Let us idealize the problem by assuming the long external bridge bond equal to the long bridge bond within the tetramer. Further let us construct from a carbon p_z orbital and a metal sp^2 hybrid orbital a sigma bond orbital. By this means the problem is reduced to a three-center four-electron problem (Figure 15b). Admittedly these are severe approximations, but they do not alter the qualitative argument to be presented. Then we can construct molecular orbitals from these sigma bond orbitals (σ_1, σ_2) and the metal p_z orbital. Figure 15b represents a molecular orbital $\phi_1 = a(\sigma_1 - \sigma_2) + b p z$, another molecular orbital would be $\phi_2 = C(\sigma_1 + \sigma_2)$. ϕ_1 is a bonding orbital and ϕ_2 is non-bonding with respect to carbon-indium-carbon interaction. The four electrons, those two-electron pairs that one would normally consider in two normal indium-carbon bonds, can be placed in the above two molecular orbitals and a closed shell diamagnetic situation

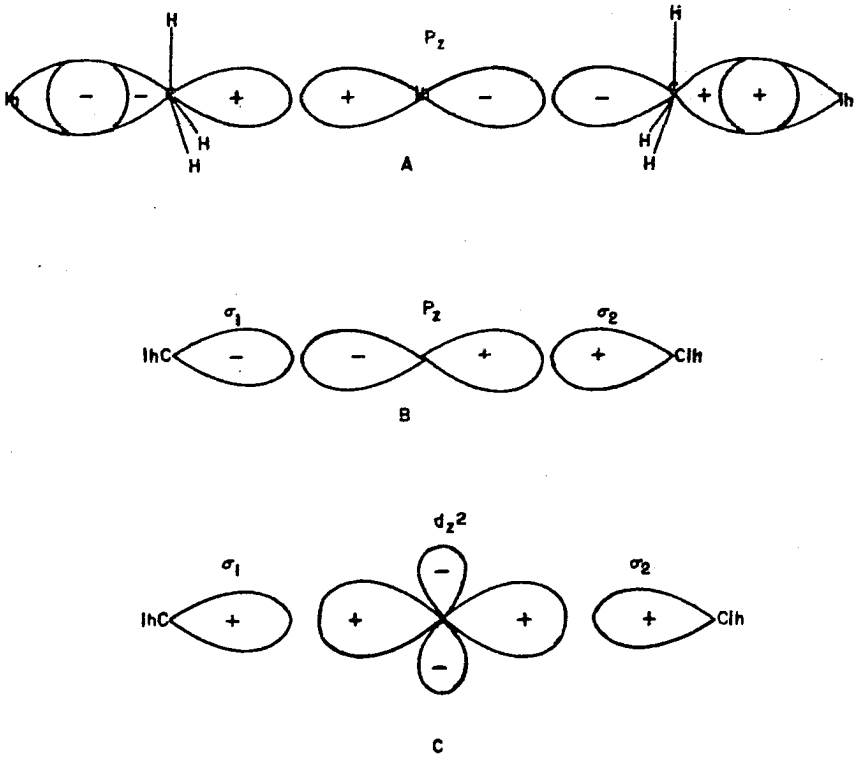

Figure 15. Bridge orbitals for trimethylindium

results. It is to be noted that this description delocalizes one of the two electron pairs. The metal atom $4d_z2$ atomic orbital is also of the correct symmetry type (Figure 15c) to form bridge orbitals, $\phi_3 = ed_z2 + f(\sigma_1+\sigma_2)$. Presumably this would be little different energetically from the non-bonding ϕ_2 orbital because of the high energy of the metal $4d_z2$ orbital. A crude correlation diagram can be drawn from this discussion as shown in Figure 16.

The bridge bonding in trimethylindium could be discussed in terms of a hyperconjugative effect. Consider the bridge bonding as before through the indium p_z orbital, but combining not with the indium-carbon bond orbitals but with carbon-hydrogen bond orbitals of the methyl groups. If we label the carbon-hydrogen bond orbitals as θ_1, θ_2, θ_3, θ_4, θ_5 and θ_6 the only combination of these orbitals that can interact with the indium p_z orbital is $(\theta_1+\theta_2+\theta_3)-(\theta_4+\theta_5+\theta_6)$. Other combinations will be non-bonding with respect to metal-carbon-hydrogen interaction because they will have nodal planes through the carbon-indium-carbon line and indium p_z cannot belong to such a representation.

In principle, at least, one should be able to distinguish between these two descriptions experimentally. To achieve maximum overlap in the hyperconjugative description the hydrogen-carbon-hydrogen angle of the bridge carbon should be quite close to tetrahedral, but to achieve maximum overlap

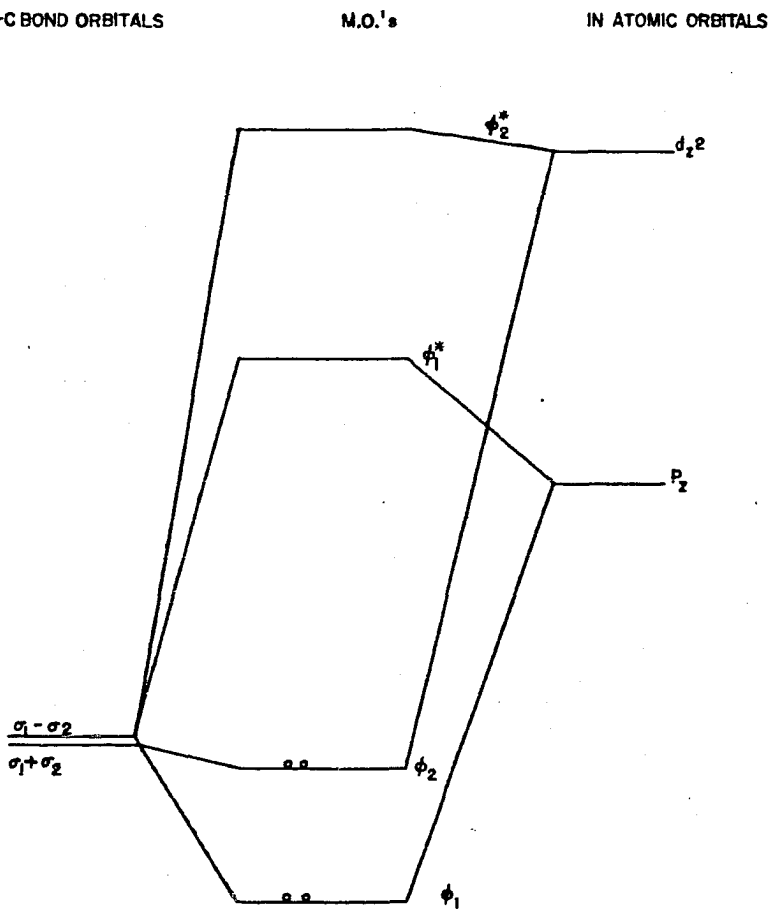

Figure 16. Crude correlation diagram for bridge orbitals of trimethylindium. Vertical scale is in energy units and horizontal scale is metal to bridge carbon distance. The diagram is meant to be purely qualitative in nature

for carbon p_z bonding the hydrogen-carbon-hydrogen angle should be distorted toward a trigonal hybridization. No doubt, the methyl group will not be completely trigonally hybridized, but the point is that a distortion toward trigonal hybridization will favor the description in terms of carbon p_z orbitals over the hyperconjugative effect.

Although the hyperconjugative description seems attractive on the surface it has some serious faults. In "classical" hyperconjugated systems such as toluene and trimethylboron it is quite reasonable to remove electrons from carbon-hydrogen bonds and displace them into carbon-carbon or carbon-boron bonds. However, the same situation does not seem to exist for trimethylaluminum. The infra-red spectra of trimethylaluminum dimer indicates the carbon-hydrogen bonds of the bridge carbon are no different from the other carbon-hydrogen bonds in the molecule. Presumably the interaction between methyl carbon-hydrogen bond orbitals and indium orbitals would follow the same trend. In other words, it is not very likely that any electron density would be removed from low energy carbon-hydrogen bond orbitals and transferred to much higher energy long bridge indium-carbon orbitals.

As the above discussion indicates, the knowledge of the configuration of the hydrogens in the bridge methyl groups would be very interesting. Unfortunately, x-ray crystallography cannot locate hydrogen atoms in the presence of

heavy metal atoms. Neutron diffraction of single crystals of trimethylindium would be capable of locating the hydrogen atoms, but even by this technique it is not a trivial problem. There are 27 hydrogen positional parameters (assuming no rotational disorder) to be determined. This would, no doubt, require three-dimensional data. Nuclear magnetic resonance would yield little information except to say that there exists at least two different types of hydrogen atoms. Infrared spectra would likewise yield little new information.

The higher homologs of trimethylindium do not appear to be associated. Triethylindium melts at -32°C., 120° below trimethylindium. This is to be expected since adjacent carbon-carbon contacts within the tetramer are 3.78Å and twice the van der Waals radius of methyl is 4.0Å. Thus, any increase in the bulk of the bridging group will exert large steric effects and tend to make the tetramer unstable. Also, increasing the bulk of the external groups tends to force the tetramers further apart making the external bridge bond less stable.

The covalent radius of thallium is not very different from indium (1.48Å and 1.44Å, respectively) and one might expect trimethylthallium to also be tetrameric. It is somewhat surprising that freezing point depression data of benzene solutions of trimethylthallium indicates a monomer (56). This is especially surprising since the melting point (38°)

of trimethylthallium is much higher than truly monomeric molecular solids such as tetramethyllead.

STRUCTURE OF GALLIUM TRIIODIDE

Preparation and Properties of Gallium Triiodide

Gallium triiodide was prepared by the method of Corbett and McMullan (57) and given to us in sealed ampules by Dr. J. D. Corbett. This method consists of reacting stoichiometric amounts of elemental gallium and iodine in a vacuum system. The compound was purified by vacuum sublimation at 150°C. The ampules were opened in a dry box and small amounts of polycrystalline gallium triiodide were transferred into capillaries. Single crystals were grown by heating the capillaries in an oil bath at the melting point of GaI_3 (210°C) and then slowly cooling the oil bath.

Pure gallium triiodide is a lemon-yellow solid melting at 210°C. It is reactive to moisture and slightly soluble in dry ethyl ether (58). The pure compound can be sublimed at atmospheric pressure but only at 345°C, at which temperature some decomposition occurs.

X-Ray Data

Crystals of several orientations were found, but data were taken only with a crystal in which the [001] direction was parallel to the capillary axis. Intensity data were taken of the h0ℓ and 0kℓ zones on the precession camera by means of timed exposures of 1, 2, ... 10, 15, 30 minutes and 1,

2, 4, 8, 16 and 48 hour duration. Weissenberg intensity data were taken of the hk0 zone by a combination of multiple film and timed exposure techniques. Lorentz and polarization corrections for the h0ℓ and 0kℓ data were made by means of the chart due to Waser (45). The hk0 Weissenberg data were corrected for Lorentz and polarization factors on the I.B.M. 650 with a program from Dr. D. H. Templeton. Higher layer photographs were also obtained to check the systematic extinctions, but no higher layer intensity data were obtained. All intensities were estimated visually.

Unit Cell and Space Group

Gallium triiodide is orthorhombic with lattice constants,

$$a = 18.29 \pm .02 \text{ Å},$$
$$b = 5.94 \pm .02 \text{ Å},$$
$$c = 6.09 \pm .02 \text{ Å}.$$

The following systematic extinctions were observed;

for hkℓ data reflections absent for $h + k = 2n + 1$

for h0ℓ data reflections absent for $h = 2n+1, \ell = 2n+1$

for 0kℓ data reflections absent for $k = 2n + 1$.

The possible space groups are then $Cmc2_1$, C2cm and Cmcm (49). With four GaI_3 molecules per unit cell $\rho_{calc.} = 4.53$ and $\rho_{obs.} = 4.15$ g/c.c. The analysis given below indicates Cmcm to be the most probable space group.

Determination of Atomic Positions

Before a Patterson projection was computed a systematic elimination of sets of crystallographic positions for each space group was carried out in so far as possible based only upon the x-ray data.

Consider first space group Cmcm with the positions as given in Table 10. The four gallium and twelve iodine atoms could be distributed in the following ways:

(1) 4 Ga (4 I) in set a,
    4 Ga (4 I) in set b,
    8 I in set c with parameters y and y'.

(2) all atoms in set c with parameters y, y', y'', y'''.

(3) 8 I in set d,
    4 Ga (4 I) in set b,
    4 Ga (4 I) in set a.

(4) 8 I in set d,
    4 Ga (4 I) in set b or a,
    4 Ga (4 I) in set c.

(5) 8 I in set d,
    4 Ga and 4 I in set c with parameters y and y'.

(6) same as (3) but 8 I in set e.

(7) same as (4) but 8 I in set e.

(8) same as (5) but 8 I in set e.

(9) same as (3) but 8 I in set f.

(10) same as (4) but 8 I in set f.

Table 10. Summary of positions and formulae for space group Cmcm

origin at center (2/m)

Number of positions	Wycoff notation	Point symmetry	Coordinates of equivalent positions (0,0,0; $\frac{1}{2},\frac{1}{2},0$) +	Conditions limiting possible reflections
16	h	1	x,y,z; $x,\bar{y},\bar{z}$; $x,y,\frac{1}{2}-z$; $x,\bar{y},\frac{1}{2}+z$; $\bar{x},\bar{y},\bar{z}$; $\bar{x},y,z$; $\bar{x},\bar{y},\frac{1}{2}+z$; $\bar{x},y,\frac{1}{2}-z$.	General: $hk\ell$: $h+k=2n$ $0k\ell$: $(k=2n)$ $h0\ell$: $\ell=2n$ $(h=2n)$ $hk0$: $(h+k=2n)$ $h00$: $(h=2n)$ $0k0$: $(k=2n)$ 00ℓ: $(\ell=2n)$ Special: as above plus
8	g	m	$x,y,\frac{1}{4}$; $\bar{x},y,\frac{1}{4}$; $x,\bar{y},3/4$; $\bar{x},\bar{y},3/4$.	No extra conditions
8	f	m	$0,y,z$; $0,\bar{y},\bar{z}$; $0,y,\frac{1}{2}-z$ $0,\bar{y},\frac{1}{2}+z$.	No extra conditions
8	e	2	$x,0,0$; $\bar{x},0,0$; $x,0,\frac{1}{2}$; $\bar{x},0,\frac{1}{2}$.	$hk\ell$: $\ell=2n$
8	d	$\bar{1}$	$\frac{1}{4},\frac{1}{4},0$; $\frac{1}{4},3/4,0$; $\frac{1}{4},\frac{1}{4},\frac{1}{2}$ $\frac{1}{4},3/4,\frac{1}{2}$.	$hk\ell$: $h,\ell=2n$ $(k=2n)$
4	c	mm	$0,y,\frac{1}{4}$; $0,\bar{y},3/4$.	No extra conditions
4	b	2/m	$0,\frac{1}{2},0$; $0,\frac{1}{2},\frac{1}{2}$.	$hk\ell$: $\ell=2n$
4	a	2/m	$0,0,0$; $0,0,\frac{1}{2}$.	$hk\ell$: $\ell=2n$

$h+k=2n$, $\ell=2n$: $F(hk\ell) = 16 \cos 2\pi hx \cos 2\pi ky \cos 2\pi\ell z$

$F(hk\ell) = F(\bar{h}\bar{k}\bar{\ell}) = F(\bar{h}k\ell) = F(h\bar{k}\ell) = F(hk\bar{\ell})$

$h+k=2n$, $\ell=2n+1$: $F(hk\ell) = -16 \cos 2\pi hx \sin 2\pi ky \sin 2\pi\ell z$

$F(hk\ell) = F(\bar{h}\bar{k}\bar{\ell}) = F(\bar{h}k\ell) = -F(h\bar{k}\ell) = -F(hk\bar{\ell})$

$$P(xyz) = \frac{8}{V_c} \sum_0^N \sum_0^N \sum_0^N F^2(hk\ell) \cos 2\pi hx \cos 2\pi ky \cos 2\pi\ell z$$

Table 10. (Continued)

$$\rho(xyz) = \frac{8}{V_c}\left[\sum_{0}^{N}\sum_{0}^{N}\sum_{0}^{N}{}^{\ell=2n} F(hk\ell)\ \mathrm{Cos}\ 2\pi hx\ \mathrm{Cos}\ 2\pi ky\ \mathrm{Cos}\ 2\pi\ell z\right.$$

$$\left. -\sum_{0}^{N}\sum_{0}^{N}\sum_{0}^{N}{}^{\ell=2n+1} F(hk\ell)\ \mathrm{Cos}\ 2\pi hx\ \mathrm{Sin}\ 2\pi ky\ \mathrm{Sin}\ 2\pi\ell z\right]$$

Summary of positions for space group C2cm

origin on 2

Number of positions	Wycoff notation	Point symmetry	Coordinates of equivalent positions (0,0,0; $\frac{1}{2},\frac{1}{2},0$) +	Conditions limiting possible reflections
8	c	1	x,y,z; x,$\bar{y}$,$\bar{z}$; x,y,$\frac{1}{2}$-z; x,$\bar{y}$,$\frac{1}{2}$+z.	General: hkℓ: h+k=2n; hk0: h+k=2n; 0kℓ: k=2n; h0ℓ: ℓ=2n,(h=2n); 00ℓ: ℓ=2n; 0k0: k=2n; h00: h=2n
4	b	m	x,y,$\frac{1}{4}$; x,$\bar{y}$,3/4.	Special: as above plus No extra conditions
4	a	2	x,0,0; x,0,$\frac{1}{2}$.	hkℓ: ℓ=2n

Summary of positions for space group $Cmc2_1$

8	b		x,y,z; $\bar{x}$,y,z; $\bar{x}$,$\bar{y}$,$\frac{1}{2}$+z; x,$\bar{y}$,$\frac{1}{2}$+z.	General: hkℓ: h+k=2n; 0kℓ: k=2n; h0ℓ: ℓ=2n;h=2n; hk0: h+k=2n; h00: h=2n; 0k0: k=2n; 00ℓ: ℓ=2n
4	a	m	0,y,z; 0,$\bar{y}$,$\frac{1}{2}$+z.	Special: as above only

(11) same as (5) but 8 I in set f.

(12) same as (3) but 8 I in set g.

(13) same as (4) but 8 I in set g.

(14) same as (5) but 8 I in set g.

Since there is not a normal decline along h00, i.e., an x parameter is indicated, combinations (1), (2), (3), (4), (5), (9), (10), (11) are eliminated from consideration. Further, combination (6) demands that, for example, for $3k\ell$ reflections should be absent when $\ell = 2n + 1$. However, these reflections are particularly strong hence, combination (6) can be eliminated. Before a Patterson projection was computed the only combinations possible for Cmcm were (7), (8), (12), (13) and (14).

Consider next space group C2cm, the possible combinations for this space group (Table 10) are as follows:

(15) all atoms in set a with x parameters x, x', x'', x'''.

(16) 4 Ga (4 I) in set a,
4 Ga (4 I) in set b,
8 I in set a with x parameters x', x''.

(17) 4 Ga (4 I) in set a,
4 Ga (4 I) in set b,
8 I in set b with xy parameters x, y; x', y'.

(18) 4 Ga and 4 I in set a with x parameters x, x',
8 I in set b with x,y parameters x'',y'',x''',y'''.

(19) 4 Ga and 4 I in set b with xy parameters x,y; x',y',
8 I in set a with x parameters x'', x'''.

(20) all atoms in set b with xy parameters x,y; x',y'; x'',
y''; x''', y'''.

(21) 8 I in set c,
4 Ga and 4 I in set a with x parameters x, x'.

(22) 8 I in set c,
4 Ga and 4 I in set b with xy parameters x,y; x',y'.

(23) 8 I in set c,
4 Ga (4 I) in set a,
4 Ga (4 I) in set b.

Combination (15) demands, e.g., for 3k ℓ the absence of reflections for which $\ell = 2n + 1$. As mentioned above, this is not so and combination (15) can be eliminated. Therefore, for space group C2cm the possible combinations were (16) through (23) before computing a Patterson projection.

Consider finally space group $Cmc2_1$, the possible combinations for this case are as follows:

(24) all atoms in set a with yz parameters, y,z; y'z'; y'',
z''; y''',z'''.

(25) 8 I in set b,
4 I and 4 Ga in set a with yz parameters y,z; y',z'.

Combination (24) does not have an x parameter and hence can be neglected. Therefore, the only possible combination for $Cmc2_1$ is (25).

The computed Patterson projection onto the (100) plane is shown in Figure 17. It is to be noted that only two peaks appeared, one at the origin and one at $y = 0$, $z = \frac{1}{2}$. Now consider this result in terms of possible combinations of positions in space group Cmcm. It is easily seen that combinations (7), (8), (12) and (13) all require peaks in the Patterson projection at $z = 1/4$. Therefore, the only possible combination for Cmcm is (14). The Patterson can be interpreted for this combination to give the eight-fold iodine a y parameter of $y = \pm 1/4$, the four-fold iodine a y parameter of $y = \pm 1/4$, and the gallium a y parameter of $y = \pm 1/4$. Another possible interpretation of the Patterson would be to make all the y parameters equal to $y = \frac{1}{2}$. However, this latter interpretation would place the gallium and four-fold iodine atoms at identically the same position and it can be ruled out on this basis.

Next, let us consider the above Patterson in terms of combinations of positions for C2cm. Combinations (16), (17), (18) and (19) can be eliminated since they demand a peak at $z = 1/4$. Further the eight-fold iodine to eight-fold iodine vectors of combination (21) give the following possibilities; $z = \frac{1}{2}$, $y = 0$; $z = \frac{1}{2}$, $y = \pm 1/4$; $z = \pm 1/4$, $y = 0$; $z = \pm 1/4$, $y = \pm 1/4$ for this projection. The second and fourth of these would require a peak at $y = 1/4$ for the four-fold iodine to eight-fold iodine and gallium to eight-fold iodine vectors.

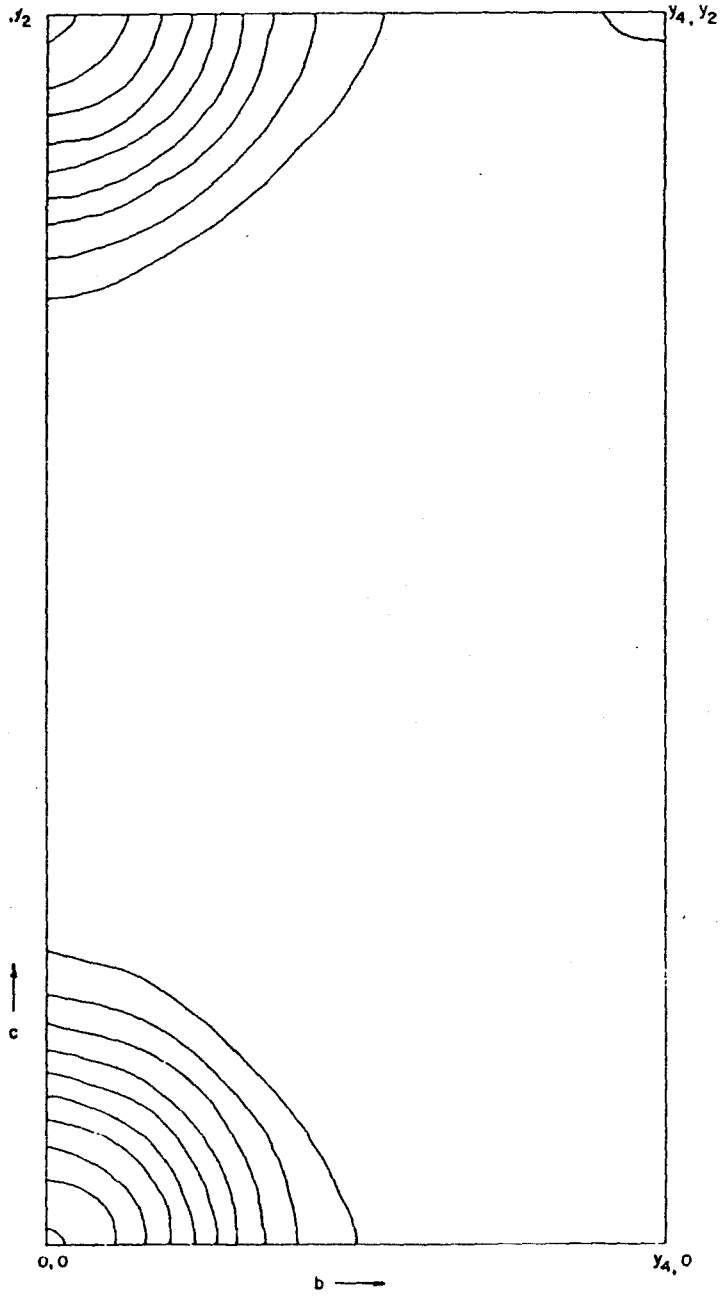

Figure 17. Patterson projection of GaI_3 onto the (100) plane

The third would require a peak at z = 1/4 for the four-fold to eight-fold vectors. The first possibility degenerates to all atoms being in set a, and this is combination (15), which has been eliminated. Since there are no peaks at z = 1/4 or y = 1/4 combination (21) is eliminated.

For combination (22) the eight-fold iodine to eight-fold iodine vectors will be the same as for (21) above with the same possible interpretations. The first two interpretations (I_8 z = $\pm \frac{1}{2}$ y = 0 ; z = $\pm \frac{1}{2}$ y = $\pm$ 1/4) can be discarded since any vector between set b and c would demand a peak at z = 1/4, and no such peak is observed. The third and fourth possibilities (I_8 z = $\pm$ 1/4, y = 0; z = $\pm$ 1/4, y = $\pm$ 1/4) degenerates to all atoms in set b which is combination (20).

Combination (23) can be ruled out since a vector between set a and set b would demand a peak at z = 1/4. Therefore, the only possible combination remaining for space group C2cm is (20), all atoms in set b.

Finally let us examine the Okℓ Patterson projection in terms of space group $Cmc2_1$. Considering combination (25), the eight-fold to eight-fold iodine vectors can be interpreted to give the parameters, (z = z, y = $\pm$ 1/4; z = z y = $\pm \frac{1}{2}$). The four-fold iodines and galliums must then have parameters; Ga z' = z y' = $\pm$ 1/4, I_4 z'' = z y'' = $\pm$ 1/4 or Ga z' = z y = $\pm \frac{1}{2}$ I_4 z'' = z y = $\frac{1}{2}$ where z could also be $\frac{1}{2}$ + z.

The computed Patterson projection onto the (010) plane is shown in Figure 18. Only two peaks are observed, one at the origin and one at z = 0, x = $\frac{13.5}{80}$. Let us now examine the three remaining possibilities (Cmcm, combination (14); C2cm, combination (20) and Cmc2, combination (25)) in terms of this projection. For Cmcm combination (14) this Patterson plus the previous one would give the following parameters:

I_8	x = .166	y = 1/4	z = ± 1/4
I_4	x = 0	y = 3/4	z = 1/4
Ga	x = 0	y = 1/4	z = 1/4

For C2cm combination (20), the 0kℓ Patterson would be identical in interpretation as for Cmcm, combination (14), i.e., all y parameters y = ± 1/4. However, this would demand more than one peak for the h0ℓ Patterson and in this way C2cm can be discarded. Further evidence for this argument will be found in the reliability index and in calculation of structure factors for unobserved reflections.

Finally for $Cmc2_1$, the h0ℓ Patterson does not allow one to distinguish between the two interpretations of the 0kℓ Patterson. However, one can examine the structure factor expression and see that for y = ½ all reflections for which ℓ = 2n + 1 must be missing or at least very weak. This is not correct and, therefore, only the first interpretation is possible.

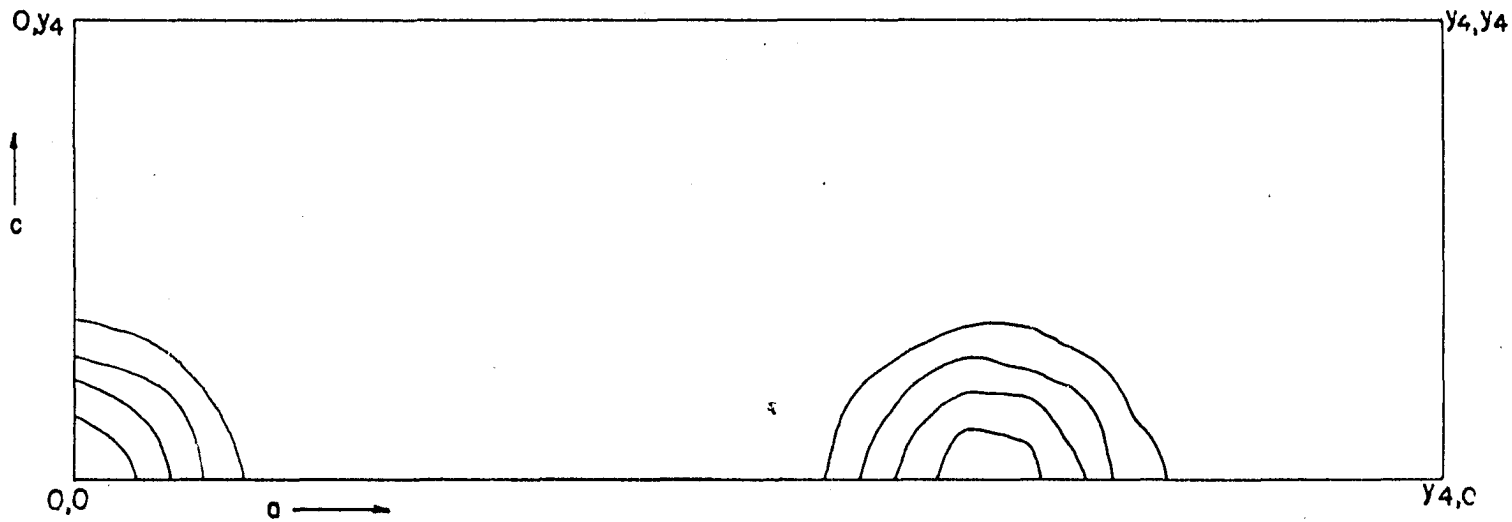

Figure 18. Patterson projection of GaI_3 onto the (010) plane

The only possible space groups are then Cmcm with the aforementioned parameters and $Cmc2_1$ with essentially the same parameters except for an additional degree of freedom in the z parameters; i.e., it will only be different from Cmcm if the z parameters of different sets are not separated by exactly $\frac{1}{2}$. This difference of not exactly $\frac{1}{2}$ would have to be quite small or it would have been detected in the Patterson projections.

Structure factors were computed, assuming space group Cmcm, for the 0k ℓ zone, and a F_c/F_o vs. $\sin^2 \theta/\lambda^2$ plot was made. The eight-fold iodine x = .166, y = 1/4, z = 1/4; four-fold iodine x = 0, y = 3/4, z = 1/4; gallium x = 0, y = 1/4, z = 1/4 were used as input data for a least squares refinement. The y parameters of all sets were pushed off y = 1/4, 3/4 collectively, in pairs and singularly and in both directions, but all y parameters refined to less than 1/4, greater than 3/4. From the structure factors calculated by the least squares analysis an electron density projection onto the (100) plane was computed and is shown in Figure 19. It is obvious from a glance at this projection that all atoms overlap considerably and accurate parameters could not be obtained from either a Fourier or a least squares analysis of this zone. However, this zone could be used to decide whether or not $Cmc2_1$ was a more probable space group than Cmcm. Attempts were made to refine the structure in space group $Cmc2_1$ by

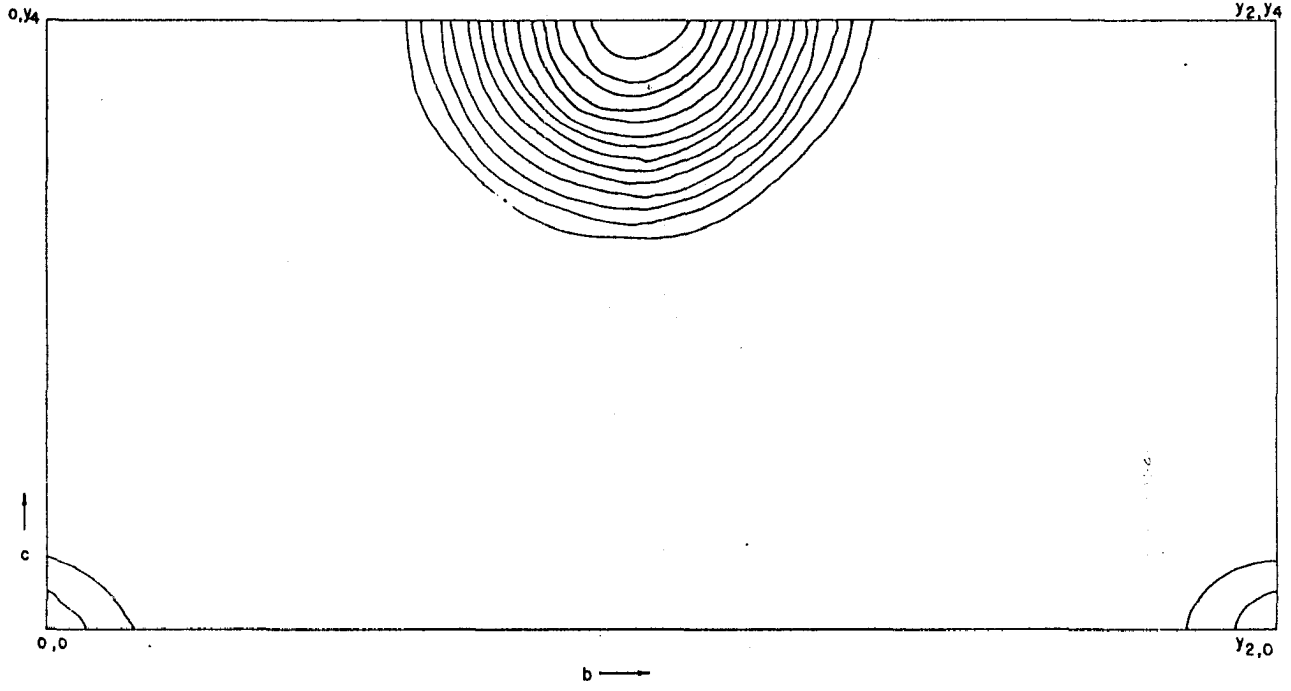

Figure 19. Electron density projection of GaI_3 onto the (100) plane

varying z parameters of all sets collectively, in pairs and singularly and in different directions from z = 1/4. However, the structure was not refined further by this means and it was decided that Cmcm was a more probable space group than $Cmc2_1$.

Structure factors, F_c/F_o plot etc., as for the $0k\ell$ zone, were computed for the $h0\ell$ zone and used as input data for least squares refinement assuming space group Cmcm. Several cycles were run and from the structure factors calculated by the least squares analysis an electron density projection onto the (010) plane was computed and is shown in Figure 20. As above, attempts were made to refine the structure as non-centrosymmetric ($Cmc2_1$). Again these attempts proved futile and gave further weight to the correctness of Cmcm as the most probable space group.

Results from the $0k\ell$ and $h0\ell$ least squares analysis were used as input data for a least squares refinement of the hk0 zone. Several cycles were computed and the structure factors calculated in the least squares computation were used to compute an electron density projection onto the (001) plane as shown in Figure 21.

It is to be noted that the four-fold iodine and gallium atoms could not be resolved in any one of the three projections. If the correct space group is Cmcm then the only parameters for these atoms which are not clearly resolved are

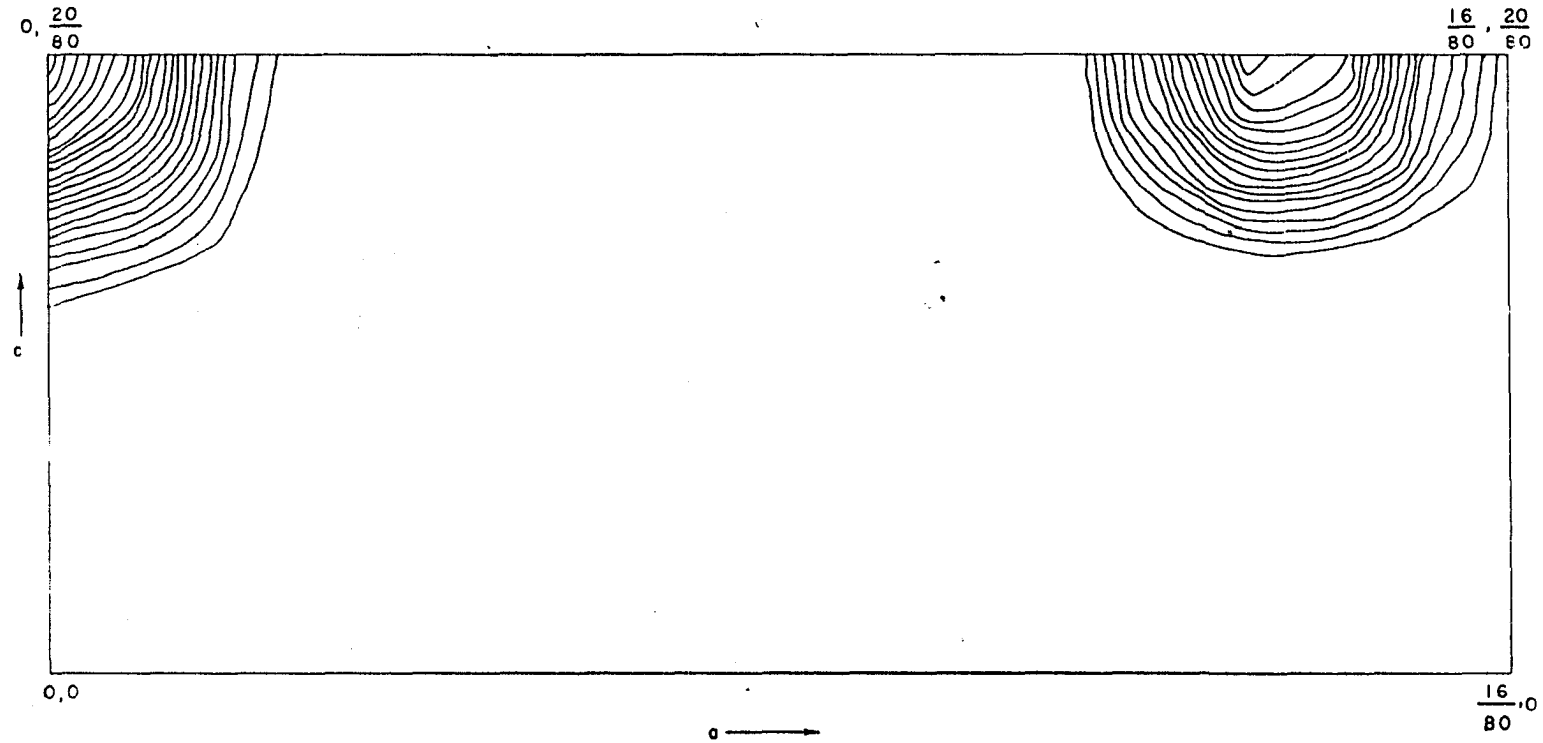

Figure 20. Electron density projection of GaI_3 onto the (010) plane. Eight-fold iodine atom is clearly resolved, but four-fold iodine and gallium atoms are not resolved along x = 0

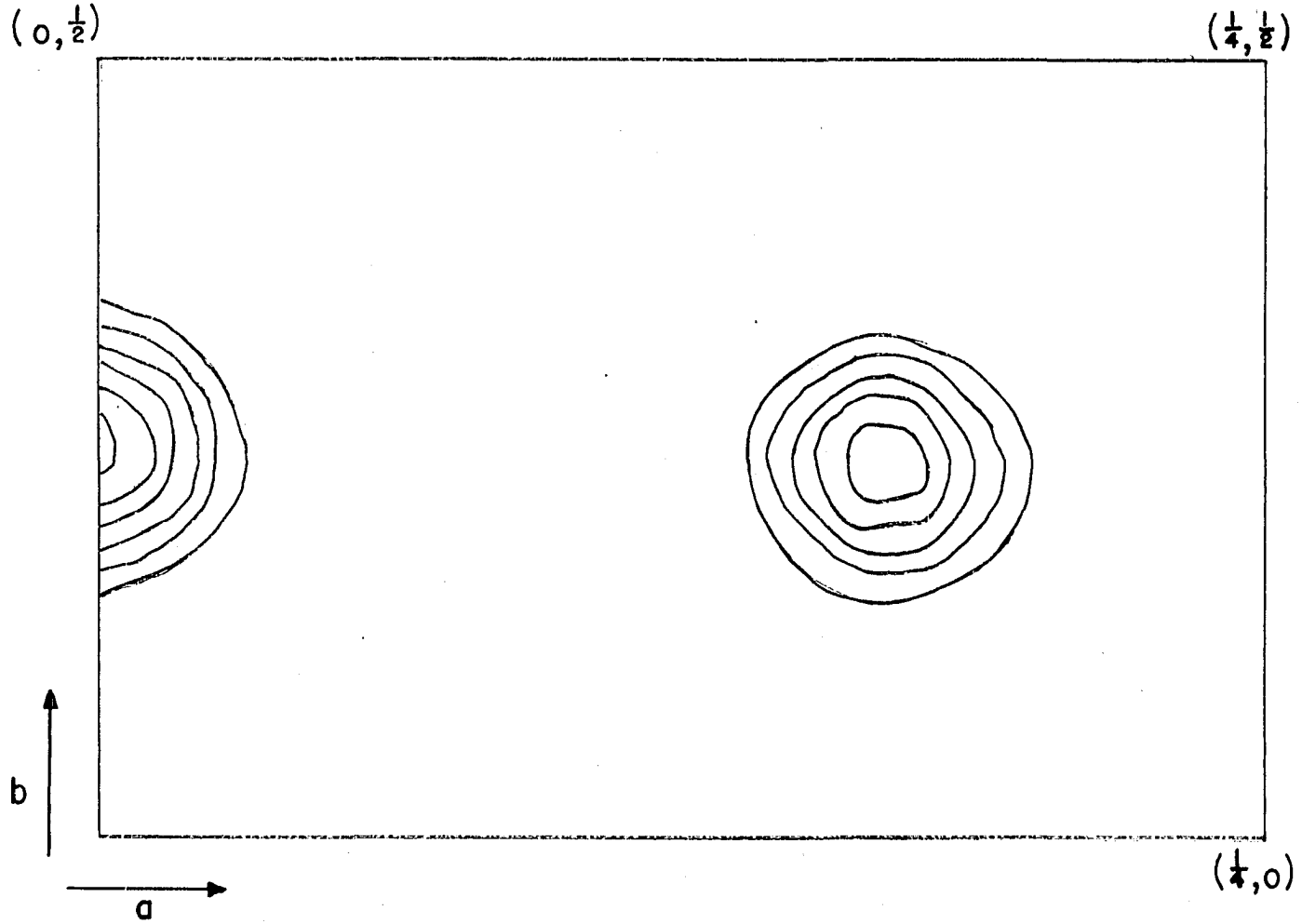

Figure 21. Electron density projection of GaI_3 onto the (001) plane. The eight-fold iodine atom is resolved but not the four-fold iodine and gallium atoms along x = 0

the y parameters for the two sets. The least squares analysis of the hk0 zone consistently refined both parameters to the same positions, given in Table 11, when they were both placed at values less than y = 1/4, greater than 3/4. The parameters of the four-fold iodine and gallium atoms given by the hk0 least squares calculation were regarded as essentially correct.

Structure factors were also computed for the unobserved reflections of the hk0 zone with the results of the above hk0 refinement, and they were all small, further supporting the correctness of the structure. This calculation also supports the correctness of the space group Cmcm and not C2cm, which would demand three additional x parameters.

The space group C2cm is ruled out by the agreement index (R_1) for the hk0 zone, Table 11. If three additional x parameters were needed one would hardly expect the agreement to be this good.

Final parameters, R factors and scale factors are given in Table 11. Bond distances are given in Table 12.

Final structure factors are tabulated in Table 13.

Unfortunately, the above least square and Fourier analysis are ambiguous in that the parameters of the four-fold iodines and the galliums can be interchanged without altering either the electron density projections or the least squares computation. This interchange would give a completely dif-

Table 11. Least squares results for GaI_3

$$R_1 = \frac{\sum_i |F_o - F_c|_i}{\sum_i |F_o|_i} \qquad R_3 = \frac{\sum_i |F_o - F_c|_i^2}{\sum_i |F_o|_i^2}$$

K (Scale factor)

Zone	R_1 %	R_3 %	
hk0	15.7	3.0	17.0
0kℓ	22.0	4.8	2.9
h0ℓ	18.0	5.5	1.4

Atom	Parameters		
	x	y	z
8-fold Iodine	.168	.224	.250
4-fold Iodine	.000	.753	.250
Gallium	.000	.245	.250
	σ x	σ y	σ z
	.003	.007	.000
	.000	.010	.000
	.000	.010	.000

Table 12. Bond distances

Atom A	Atom B	Distance A-B (Å)
Ga	4-fold I (almost directly above or below along c)	3.04 ± .02
Ga	4-fold I (directly along b)	3.02 ± .08
Ga	4-fold I (directly along b) (next unit cell)	2.92 ± .08
Ga	8-fold I (at same Z value as Ga)	3.07 ± .05
8-fold I	8-fold I (distance between sleets)	4.29 ± .07
8-fold I	8-fold I (along sleet)	4.05 ± .07
8-fold	8-fold I (along sleet)	4.50 ± .07
Ga	Ga (directly along b)	4.30 ± .08
Ga	Ga (directly along b) next unit cell	4.21 ± .08
4-fold I	8-fold I (closest)	4.32 ± .07
4-fold I	4-fold I (directly along b)	4.28 ± .08
4-fold I	4-fold I (directly along b) next unit cell	4.23 ± .08

Table 13. Final structure factors

All structures positive unless otherwise indicated

Indices	kF_o	$F_c e^{-M}$
0kℓ zone		
(0k0)		
2	57.8	-68.4
4	41.1	32.4
6	11.6	11.1
8	6.9	2.6
(0k2)		
0	60.0	-71.4
2	71.9	54.7
4	22.5	-27.0
6	15.7	9.4
(0k4)		
0	43.2	38.4
2	21.3	-30.7
4	20.6	16.3
6	8.1	5.9
(0k6)		
0	11.9	-16.3
2	15.9	13.4
4	7.4	7.4
(0k8)		
0	7.2	5.5
(0k1)		
2	9.2	-11.9
4	9.2	-12.1
6	6.9	6.9
(0k3)		
2	6.4	- 7.9
4	7.5	- 8.6
6	7.8	5.1
h0ℓ zone		
(00ℓ)		
2	29.4	-37.4
4	36.0	23.4
6	7.6	-13.1
(60ℓ)		
0	29.3	37.4
2	30.1	-31.4
4	20.4	20.5
6	11.3	-11.8
(10·0·ℓ)		
0	5.4	6.2
2	7.6	- 6.0
(12·0·ℓ)		
0	26.9	23.4
2	18.9	-20.5
4	15.9	14.6
6	5.9	- 8.9
(18·0·ℓ)		
0	15.7	13.1
2	11.1	-11.8
4	9.4	8.9
6	4.8	- 5.9
8	3.6	3.6
(20·0·ℓ)		
0	5.8	5.1
0	6.2	6.9
2	8.0	- 6.4
hk0 zone		
(h00)		
6	64.8	73.2
10	6.9	8.4
12	41.9	42.4
18	22.0	20.5
24	8.5	8.4
(h10)		
9	9.3	- 4.6

Table 13. (Continued)

Indices	kF_o	$F_c e^{-M}$	Indices	kF_o	$F_c e^{-M}$
(h20)			12	24.5	19.9
4	8.8	-11.1			
6	71.1	-57.5	(h50)		
10	10.2	- 7.1	9	11.9	- 8.8
12	35.5	-34.8			
18	14.1	-17.2	(h60)		
			6	21.6	-11.9
(h30)					
1	8.7	- 9.2	(0k0)		
3	14.6	13.3	2	63.3	-70.1
5	14.8	- 8.7	4	48.3	35.8
			6	13.6	-13.6
(h40)					
6	29.1	30.6			

ferent structure. Arguments in favor of the structure given initially are presented below.

Discussion

As mentioned above, the two-dimensional x-ray data alone cannot decide between two possible structures. Specifically, one can interchange the four-fold iodine and gallium sets and the aforementioned analysis remains unchanged. The two possible structures will be individually discussed as the "preferred" structure and the "alternate" structure and the reasons for assuming the "preferred" one to be correct will be given.

"Preferred" structure

The preferred structure consists of infinite sheets made up of a rectangular, almost square, array of alternate gallium and iodine atoms. Each gallium atom has, in addition to the four iodine atom neighbors in the array, two neighboring iodine atoms above and below the plane formed by the array. This gives each gallium atom a coordination number of six (Figure 22).

The rectangular array is parallel to the (100) plane and the gallium-iodine distance in the [001] direction is $\frac{1}{2}$ c or 3.04Å. In the [010] direction the gallium-iodine distance alternates between 2.92 and 3.02Å. The two external (external to the array) iodine neighbors of the gallium atom have a gallium iodine distance of 3.07Å and they are separated by 4.29Å (van der Waals distance) from the corresponding iodine atoms of an adjacent array (Figure 23). This should produce easy (100) cleavage.

The gallium-iodine distances in the array are all about 3.0Å. Since, the sum of the ionic radii of gallium and iodide ions is 2.77Å and the sum of the covalent radii is 2.54Å, the distances tend to favor ionic bonding. However, the observed distances are almost 0.3Å longer than even the sum of the ionic radii.

A crude estimate of the bond energy of a gallium-iodine electron pair bond can be obtained from the heat of formation

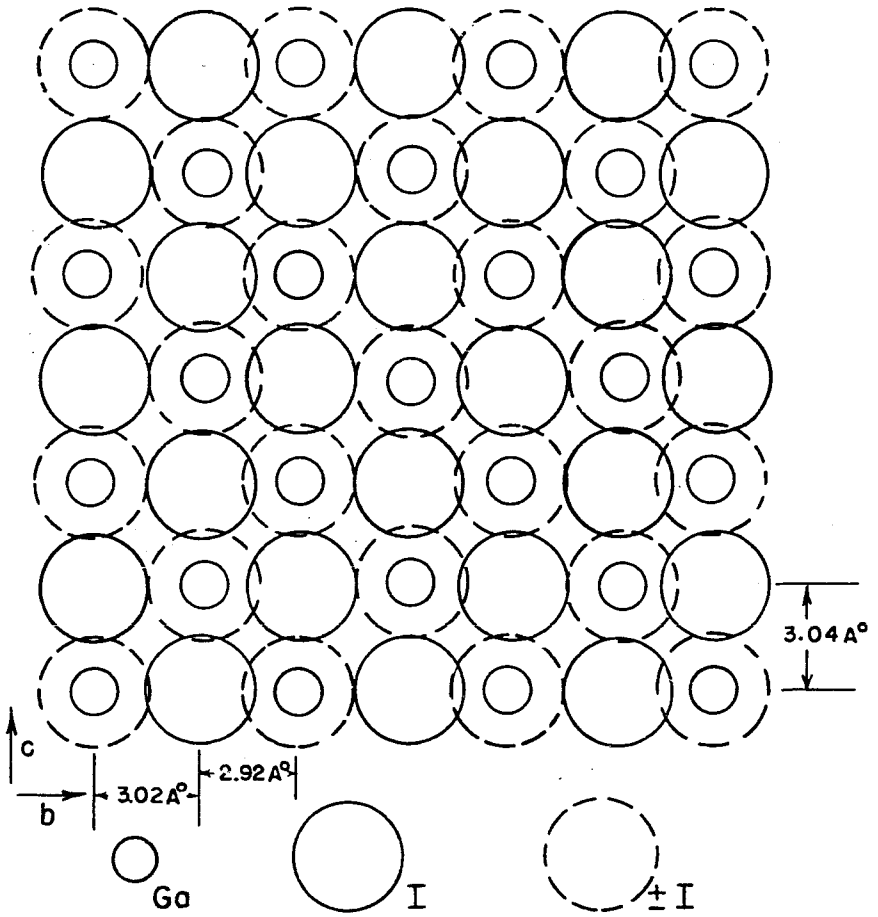

Figure 22. Sheet structure of GaI_3

Full circles represent gallium and iodine atoms in the rectangular array in the plane of the paper. Dotted circles represent iodine atoms external to the array above and below the plane of the paper

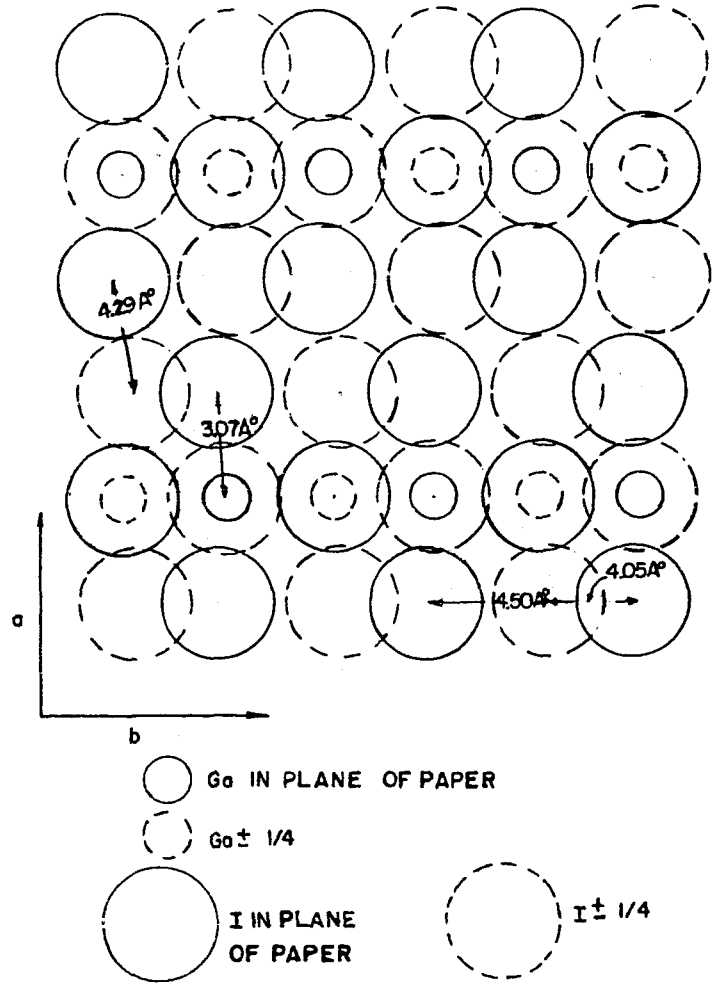

Figure 23. End on view of the sheet structure of GaI_3
The sheet is defined by the gallium atoms in the horizontal line. The distance between the closest external iodine atoms of neighboring arrays is 4.29Å. Distance between neighboring external iodine atoms along the array is either 4.50 or 4.05Å

of crystalline GaI_3 from the elements in their standard states. Using the tabulated values; of the heat of formation of crystalline GaI_3, [-51.2 Kcal./mole (59)], the heat of sublimation of Ga (65.14 Kcal./mole), the heat of sublimation plus the heat of dissociation of iodine (25.48 Kcal./mole), the heat of vaporization of Ga_2I_6 (27 Kcal./mole) and a reasonable estimate of the heat of fusion of crystalline GaI_3 (10 Kcal./mole) one easily calculates the bond energy of a Ga-I electron pair bond. This bond energy was found to be 40 Kcal./mole, assuming eight electron pair bonds per dimer. The bridge and external bonds of the dimer are undoubtedly different, but no data exist to differentiate between them.

If one assumes the p_x and p_y orbitals of the iodine atom to be in the plane of the array and the p_z orbital perpendicular to the array then each iodine could form a $\frac{1}{2}$ electron pair bond to a gallium atom. This would mean, on the basis of the calculation of the previous paragraph, that the bond energy of a gallium-iodine bond in the array would be approximately 20 Kcal./mole. The energy of the external bond, considering it as an electron pair bond, would then be 40 Kcal./mole. One would anticipate that the external Ga-I bond would be 0.18Å shorter, if Pauling's rule is used (60), than the Ga-I bonds in the array. It is puzzling, indeed, that this shortening is not observed. Since all the iodine atoms are separated by distances very close to the van der

Waals radius of iodine it may well be that a compromise has been reached at the observed distance between stronger bonds and larger van der Waals repulsive energies. However, it is somewhat difficult to see how the van der Waals forces can be large enough to distort a relatively strong bond of 40 Kcal./mole as much as is observed.

As mentioned in the Introduction, Barnes and his co-workers have measured the nuclear quadrupole resonance spectra of polycrystalline gallium triiodide. The gross aspects of the iodine resonance consist of two lines separated by 1 per cent of the resonance frequency and a third line about 15-20 per cent of the resonance frequency lower. The nuclear quadrupole resonance of Ga^{69} and Ga^{71} have also been observed. On the basis of these resonances it has been assumed that iodine bridged dimeric molecules exist in the solid. The first two lines of the iodine spectrum have been attributed by Barnes et al to the terminal iodine atoms of the dimer. The 1 per cent splitting has been attributed to crystallographically independent, though chemically similar, atoms. The asymmetry parameter (η) of the so called bridge iodines has been computed to be 23.7 ($\eta = \frac{q_{xx}-q_{yy}}{q_{zz}}$ where $q_{xx} = \partial^2 V / \partial x^2$). The asymmetry parameters of the so called terminal iodines have been computed to be 0.9 and 2.8. The latter small asymmetry parameters were attributed by Barnes to cylindrically symmetrical σ bonds.

The I-Ga-I bridge angle, assuming dimers in crystalline GaI_3, was computed to be 82° from the nuclear resonance data. The results of our x-ray investigation clearly indicate an angle of 90° for the I-Ga-I angle in the crystalline array. It is not at all clear whether or not the distortion of the square array is sufficient to give the observed field gradient and asymmetry parameters. For crystalline GaI_3 the 1 per cent splitting cannot be attributed to crystallographically independent terminal atoms since the external iodine atoms belong to a special eight-fold set and all other iodines are in the array. This small splitting could possibly arise from the external iodine atoms that are separated by 4.05Å, i.e., an iodine-iodine contact interaction. In crystalline iodine a similar splitting and interaction occurs (61), but here the closest intermolecular distance is 3.6Å.

Barnes (62) has also observed that the Ga^{69} and Ga^{71} resonances disappear at liquid nitrogen temperatures, but the so called bridge and terminal iodine resonances remain. It is not at all clear from the structure what happens at liquid nitrogen temperatures that would account for this phenomenon, except possibly all y parameters changed to exactly 1/4 or 3/4. This would increase the local symmetry about the gallium atom, but it would also seem to increase the symmetry about the iodine atom, within the array.

It is a distinct possibility that the nuclear quadrupole resonance experiments are much too sensitive to electronic environments to be capable of ascertaining gross geometric features in the solid state. For example, the crystal structure of $CrCl_3$ and $AlCl_3$ are very much alike except that the local symmetry about an aluminum atom is lower than about the Cr atom. Their nuclear quadrupole resonance spectra are, however, remarkably different. In solid $AlCl_3$ neither the chlorine nor the aluminum resonances have been found in spite of experiments with large pure samples. On the other hand, both the chromium and the chlorine resonances were easily detected. This is, indeed, a disturbing situation for anyone who hopes to decide molecular or ionic geometry by correlating nuclear quadrupole resonances.

Disastrous as the above may seem for the nuclear spectroscopist, it need not be so. X-ray crystallography can locate atoms and decide molecular geometry but can ascertain little concerning finer details of electron distribution and chemical bonding. It seems that a cooperative spirit between the nuclear spectroscopist and the x-ray crystallographer might prove very informative to both groups.

"Alternate" structure

The alternate structure would consist of interchanging the four-fold iodine and gallium positions. This would leave

the array unchanged but would make the external iodine atoms nearest neighbors to the iodine atoms in the array as in the "preferred" structure.

This situation is not very likely chemically, for if one wishes to say that a good share of the bonding is ionic then this would place three relatively negative charges close together. This could give each iodine atom in the array six nearest neighbors, two of which would be iodines and the other four galliums. Gallium would then have a coordination number of only four, and the configuration about it would be square planar. In the circumstances it is deemed justifiable to drop consideration of the alternate structure. It should be added that in principle, at least, the two structures could be differentiated, but the overlapping of peaks is sufficient to make this, in practice, difficult if not impossible with only two-dimensional projections.

BIBLIOGRAPHY

1. Lewis, G. N., J. Am. Chem. Soc., 38, 762 (1916).

2. Rundle, R. E., J. Phys. Chem., 61, 45 (1957).

3. Rundle, R. E., Acta Cryst., 1, 180 (1948).

4a. Rundle, R. E., J. Am. Chem. Soc., 69, 1327 (1947).

4b. Rundle, R. E., J. Chem. Phys., 17, 671 (1949).

5a. Longuet-Higgins, H. C. and Bell, R. P., J. Chem. Soc., 1943, 250.

5b. Longuet-Higgins, H. C., Quart. Rev., 11, 121 (1957).

5c. Pitzer, K. S., J. Am. Chem. Soc., 67, 1126 (1945).

6. Price, W. C., J. Chem. Phys., 16, 894 (1948).

7. Hedberg, K. and Schomaker, V., J. Am. Chem. Soc., 73, 1482 (1951).

8. Pitzer, K. S., J. Am. Chem. Soc., 68, 2204 (1946).

9. Burg, A., J. Am. Chem. Soc., 69, 747 (1947).

10. Ogg, R. A., Jr., J. Chem. Phys., 22, 1933 (1954).

11a. Longuet-Higgins, H. C., J. Chem. Phys., 46, 275 (1949).

11b. Eberhardt, W. H., Lipscomb, W. N. and Crawford, B., J. Chem. Phys., 22, 989 (1954).

12. Hamilton, W. C., Proc. Roy. Soc. (London) A235, 395 (1956).

13. Lipscomb, W. N., J. Chem. Phys., 22, 985 (1956).

14a. Lipscomb, W. N., Eriks, K. and Schaeffer, R., J. Chem. Phys., 22, 754 (1954).

14b. Lipscomb, W. N., Howell, P. A., Wheatley, P. J. and Dickerson, R. E., J. Chem. Phys., 27, 200 (1957).

15. Harker, D., Lucht, C. M. and Kasper, J. S., Acta Cryst., 3, 436 (1950).

16. Lipscomb, W. N., J. Chem. Phys., 25, 38 (1956).

17. Rundle, R. E. and Sturdivant, J. H., J. Am. Chem. Soc., 69, 1561 (1947).

18. Eyring, H., Walter, J. and Kimball, G. E. Quantum Chemistry. John Wiley and Sons, Inc. New York, 1949.

19. Pitzer, K. S. and Gutowsky, H., J. Am. Chem. Soc., 68, 2204 (1946).

20. Longuet-Higgins, H. C., J. Chem. Soc., 1946, 139.

21. Lewis, P. H. and Rundle, R. E., J. Chem. Phys., 21, 986 (1953).

22. Snow, A. I. and Rundle, R. E., Acta Cryst., 4, 348 (1951).

23. Dennis, L. M. and Patnode, J., J. Am. Chem. Soc., 54, 182 (1932).

24. Pauling, L. Nature of the Chemical Bond. 2nd ed. Cornell University Press. Ithaca, New York, 1949.

25. Dennis, L. M., Work, R. W., Rochow, E. G. and Chamot, E. M., J. Am. Chem. Soc., 56, 1047 (1934).

26. Pauling, L. and Laubengayer, A. W., J. Am. Chem. Soc., 63, 480 (1941).

27. Palmer, K. J. and Elliot, N., ibid, 60, 1852 (1938).

28. Rundle, R. E. and Lewis, P. H., J. Chem. Phys., 20, 132 (1952).

29. Templeton, D. H. and Clark, E. S., International Congress of International Union of Crystallography. Abstracts of the Communications 4, 57 (1957).

30. Buraway, A., Gibson, C. S. Hampson, G. C. and Powell, H. M., J. Chem. Soc., 1936, 1635.

31. Ketelaar, J. A. A., Renes, P. A. and MacGillavry, C. H., Rec. trav. chim., 66, 501 (1947).

32. Wells, A. F., Z. Krist., 100, 189 (1938).

33. Gerdig, H. and Smit, E., Z. Physik. Chem., B50, 171 (1941).

34. Renes, P. A. and MacGillavry, C. H., Rec. trav. Chim., 64, 275 (1945).

35. Barnes, R. G. and Segel, S. L., Bull. of the Am. Phys. Soc., Series 2, 1, 282 (1956).

36. Barnes, R. G. and Segel, S. L., J. Chem. Phys., 25, 578 (1956).

37. Sidgewick, N. V. Chemical Elements and Their Compounds. Oxford University Press. London, England, 1950.

38. Stevenson, D. P. and Schomaker, V., J. Am. Chem. Soc., 64, 2514 (1941).

39. Templeton, D. H. and Clark, E. S., University of California Radiation Laboratory, Report 2531, 1954 .

40. Amma, E. L., Iowa State College, Chemistry Department, Ames, Iowa. Unpublished research on the crystal structure of $InBr_3$ (1956).

41. Barnes, R. G., Segel, S. L., Bray, P. J. and Casabella, P. A., J. Chem. Phys., 26, 1345 (1957).

42. Greenwood, N. N. and Worrall, I. J., J. Inorg. Nucl. Chem., 3, 357 (1957).

43a. Segel, S. L. Ames, Iowa. Private Communication. May 1957.

43b. Barnes, R. G. Ames, Iowa. Private Communication. September 1957.

44. Coates, G. E. and Whitcombe, R. A., J. Chem. Soc., 1956, 3351.

45. Waser, J., Rev. Sci. Instrum., 22, 563 (1951).

46. Cochran, W., J. Sci. Instrum., 25, 253 (1948).

47. Phillips, D. C., Acta Cryst., 9, 819 (1956).

48. Buerger, M. J. X-Ray Crystallography. John Wiley and Sons, Inc. New York, 1942.

49. International Tables for X-Ray Crystallography. Vol. 1 The Kynoch Press. Birmingham, England. 1952.

50. International tabellen zur bestimmung von Kristalstructuren. Vol. 2. Gebruder Borntraeger. Berlin, Germany. 1935.

51. Booth, A. D. Fourier Technique in X-Ray Organic Structure Analysis. Cambridge University Press. Cambridge, England. 1948.

52. Berghuis, J., Hannappel, H., Ijbertha, M., Potters, M., Loopstra, B. O., MacGillavry, C. H. and Veenendaal, A. L., Acta Cryst., 8, 478 (1955).

53. Lipson, H. and Cochran, W. The Determination of Crystal Structures. G. Bells and Sons. London, England, 1953.

54. Cruickshank, D. W. J., Acta Cryst., 2, 65 (1949).

55a. Ibers, J. A. and Cromer, D. T. International Congress of International Union of Crystallography. Abstracts of the Communications 4, 21 (1957).

55b. Hughes, E. W., J. Am. Chem. Soc., 63, 1737 (1941).

56. Gilman, H. and Jones, R. G., J. Am. Chem. Soc., 68, 517 (1946).

57. Corbett, J. D. and McMullan, R. K., J. Am. Chem. Soc., 77, 4217 (1955).

58. Wood, R. E. and Ritter, H. L., J. Am. Chem. Soc., 74, 1760 (1952).

59. Rossini, F. D., Wagan, D. D., Evans, W. H., Levine, S. and Jaffe, I., U.S. Dept. of Commerce. Circular 500 of the National Bureau of Standards. 1952.

60. Pauling, L., J. Am. Chem. Soc., 69, 542 (1947).

61. Watkins, G. D. and Walker, R. M., Bull. Am. Phys. Soc., Ser. 2, 1, 11 (1956).

62. Barnes, R. G. Ames, Iowa. Private Communication. November, 1957.

ACKNOWLEDGMENTS

The author wishes to express his deepest gratitude to Dr. R. E. Rundle for his advice, interest and many helpful discussions, not only in this research but also in problems of general interest.

The author is also grateful to Mr. D. R. Fitzwater for his work on the programming of the I.B.M. 650 for much of the computations.

A debt of gratitude is due also to former and some of the present members of Dr. Rundle's research group from whom much valuable knowledge of crystallography has been obtained.

He is also grateful to Mr. H. F. Hollenbeck for his aid with the drawings in this work.

The author is most grateful for the encouragement and faith given by his wife throughout the course of this research. He is also grateful for her efforts in typing the rough draft of this thesis.